



HAL
open science

Hierarchical modeling of heterogeneous structures driven by a modeling error estimator

Mouad Fergoug, Augustin Parret-Fréaud, Nicolas Feld, Basile Marchand,
Samuel Forest

► **To cite this version:**

Mouad Fergoug, Augustin Parret-Fréaud, Nicolas Feld, Basile Marchand, Samuel Forest. Hierarchical modeling of heterogeneous structures driven by a modeling error estimator. *Computer Methods in Applied Mechanics and Engineering*, 2024, 418 (Part B), pp.116529. 10.1016/j.cma.2023.116529 . hal-04263893

HAL Id: hal-04263893

<https://hal.science/hal-04263893>

Submitted on 29 Oct 2023

HAL is a multi-disciplinary open access archive for the deposit and dissemination of scientific research documents, whether they are published or not. The documents may come from teaching and research institutions in France or abroad, or from public or private research centers.

L'archive ouverte pluridisciplinaire **HAL**, est destinée au dépôt et à la diffusion de documents scientifiques de niveau recherche, publiés ou non, émanant des établissements d'enseignement et de recherche français ou étrangers, des laboratoires publics ou privés.

Hierarchical modeling of heterogeneous structures driven by a modeling error estimator

Mouad Fergoug^{1,2*}, Augustin Parret-Fréaud¹, Nicolas Feld¹, Basile Marchand²,
Samuel Forest²

¹*Safran Tech, Digital Sciences & Technologies Department, Rue des Jeunes Bois, Châteaufort,
78114 Magny-Les-Hameaux, France*

²*MINES Paris, PSL University, MAT – Centre des matériaux, CNRS UMR 7633, BP 87 91003
Evry, France*

Abstract

Homogenized models are widely used in multiscale analysis for their computational efficiency, but they often fail to provide sufficient accuracy in regions exhibiting high variations in the solution fields. One way to address this limitation is to adaptively couple the homogeneous model with a full field, heterogeneous one in designated zones of interest. Within the framework of finite-element based higher-order asymptotic homogenization, this work introduces a modeling error estimator in order to detect regions where refining the material model is necessary. We also analyze the competition between discretization and modeling errors. We finally propose a multi-scale enhancement of the classical displacement-based submodeling technique in order to adequately couple the homogeneous and heterogeneous domains. The promise of the proposed methods and the overall associated strategy is illustrated on various numerical examples of elastic fiber-matrix composites.

Keywords: asymptotic homogenization, modeling error, hierarchical modeling.

*Corresponding author

Email address: augustin.parret-freaud@safrangroup.com (Augustin Parret-Fréaud¹)

1. Introduction

Analyses of heterogeneous structures are conventionally performed using effective or homogenized material properties, instead of explicitly taking into account each material phase and the geometrical arrangements of the microstructure. These effective properties are usually obtained by homogenization methods, which can be broadly divided into two main categories: closed-form (or analytical) methods and computational methods.

Asymptotic homogenization, firstly introduced in the theoretical work of [Sanchez-Palencia \(1983\)](#) and [Bensoussan et al. \(2011\)](#), is one of the most rigorous closed-form homogenization approaches available in the literature. It is based on the assumption of spatial periodicity of the microstructure where the unit-cell defines the Representative Volume Element (RVE) without any ambiguity. This method consists in using asymptotic expansions of the mechanical fields of the full-scale problem in order to split it into a decoupled set of microscale unit-cell problems and a macroscale problem. Solving the former allows one to compute the effective properties of the equivalent homogeneous medium but also to estimate, by a localization process, local fields within the material. Asymptotic homogenization, as an engineering tool, has been explored in the seminal works of Kikuchi and coworkers ([Guedes and Kikuchi, 1990](#); [Hollister and Kikuchi, 1992](#); [Terada and Kikuchi, 1995](#)) where the finite element method has been used to solve the unit-cell problems to compute equivalent material properties, as well as local fields estimation. Such multiscale computational analyses have been conducted by [Ghosh et al. \(1995, 2001\)](#) where the asymptotic homogenization theory has been combined with the Voronoi cell finite element method (VCFEM) to study elastic and elasto-plastic material behavior. Fish and coworkers ([Fish et al., 1994b](#); [Fish and Belsky, 1995](#); [Fish and Yu, 2001](#)) have used asymptotic homogenization to develop a multigrid method for the analysis of pe-

riodic materials and to account for the damage phenomena occurring at different scales. Recent works resort to asymptotic homogenization in a wide range of engineering problems, *e.g.* to study metamaterial behavior (Yang et al., 2019, 2020; Abali and Barchiesi, 2020; Abali et al., 2022; Yang et al., 2022), to optimize structures (Suzuki and Kikuchi, 1991; Sigmund, 1995; Hassani and Hinton, 2012), and to evaluate localized stiffness degradation (Visrolia and Meo, 2013). Generalized non-linear problems are more often tackled using so-called computational homogenization methods (Moulinec and Suquet, 1998; Feyel and Chaboche, 2000; Kouznetsova et al., 2001, 2002; Miehe and Koch, 2002), which have the same basic structure as other asymptotic homogenization approaches, but rely on an incrementally linearized multiscale analysis, alternating macro-problem resolution to recover the global balance and micro-problem analyses – often heavily parallelized – to recover local stresses and Jacobians. The reader is referred to Kanouté et al. (2009) for a thorough review of homogenization methods. In this article, we use asymptotic homogenization for multiscale linear behavior analyses. Therefore, only periodic heterogeneous structures are considered.

Conventional or first-order asymptotic homogenization, which considers only the first term in the asymptotic expansion, works well for cases with a complete separation of scales. This assumption is only valid when the scale of the microstructure or microstructural fluctuations are much smaller than the characteristic dimensions of the macrostructure. For weak separation of scales, however, it generally becomes inaccurate (Ameen et al., 2018). One solution to overcome this limitation is to keep higher-order terms in the series expansion. Indeed, Boutin (1996) shows that higher-order terms in asymptotic homogenization introduce successive gradients of macroscale strain and tensors characteristic of the microstructure, which result in introducing a non-local effect in the material behavior. Therefore, asymptotic homoge-

nization may offer a better estimate of local fields, even in cases of a weak separation of scales, by a higher-order localization process. Nevertheless, the construction of a solution at the vicinity of the boundaries remains beyond the capabilities of this method due to the loss of periodicity assumption in these regions, unless a boundary layer correction is applied. In [Fergoug et al. \(2022b\)](#) a FEM numerical framework has been proposed to perform a higher-order localization process associated with a general boundary layer correction method. This work is limited to the assumption that both the heterogeneous microscale mesh, constructed by translating the unit-cell, and the overall macroscale mesh are identical, which can be computationally prohibitive. In the present article, we propose an extension of the aforementioned work to deal with different coarser macroscale meshes, requiring less computation time than Direct Numerical Simulations (DNS, *i.e.* when the geometry of the microstructure is explicitly described in simulations). As a result, local fields corrected at the boundaries needed, for example, to predict damage initiation, will be estimated on the coarse macroscale mesh.

Numerical simulations of heterogeneous structures depend on several factors such as the characteristics of the microstructure, the domain of interest, and the applied loads as well as the targeted accuracy and the objective of the simulation. Consequently to avoid a DNS, there is a need to *adaptively* select the appropriate scale for each domain of interest. Toward this end, the concept of *hierarchical modeling* was introduced to couple a multilevel material model in the same simulation. This process of adaptivity is usually steered by criteria used to detect areas where refining the material model is necessary. These criteria can be physically oriented, for example, based on the level of stress, strain or damage ([Ghosh et al., 2001](#)) or mathematically oriented by using the macroscale discretization error or the modeling error ([Zohdi et al., 1996](#); [Fish et al., 1994a](#); [Ghosh et al., 2007](#); [Temizer and Wrig-](#)

gers, 2011; Vernerey and Kabiri, 2012). The non-exhaustive representative works that have treated the subject of adaptivity are as follows:

- Zohdi et al. (1996) and Oden and Zohdi (1997) have initiated a hierarchical modeling strategy based on the estimation of a global *modeling error*, which quantifies the error induced by replacing the heterogeneous material with a homogeneous one. Based on the observation that global estimates can be insensitive to *local* features such as stress concentrations or average strains, Oden and Vemaganti (1999, 2000) have proposed an extension of the modeling error to quantities of interest. This error estimation and adaptivity process have been extended to nonlinear problems by Oden et al. (2001). A disadvantage of this class of methods is that it needs access to the full microscale material fluctuations, and the modeling error estimation is thus conducted through an integral over the corresponding heterogeneous domain, which can be computationally prohibitive.
- Fish and coworkers (Fish and Markolefas, 1993; Fish et al., 1994a; Fish and Belsky, 1995; Fish and Shek, 2000) have proposed the adaptive s-method, a coupling strategy of the macroscale with the microscale of an underlying periodic microstructure at a region of interest identified by *multiscale reduction error estimators/indicators* derived from asymptotic homogenization. The limitation of this method is that it does not take into account the boundary layer effect, which is predominant in many industrial applications.
- Ghosh and coworkers (Ghosh et al., 2001; Raghavan and Ghosh, 2004; Raghavan et al., 2004; Ghosh et al., 2007) have suggested an adaptive multi-level methodology to create a hierarchy of computational sub-domains with a varying

resolution, from homogenized formulations to explicit microstructural modeling. The macroscale computations are done by conventional FEM models while the VCFEM is used for micromechanical analysis. The switching criteria from one level to another can be associated with the gradients of macroscale variables (*e.g.* stress, strain, or strain energy) or the evolution of microscale damage. This method has addressed damage evolution in composites accurately and efficiently.

In this article, we present a novel modeling error estimation based on a higher-order localization process derived from asymptotic homogenization. The main idea of the proposed estimation is to quantify the terms neglected by conventional first-order homogenization, necessary to capture the gradients of the macroscale field in case of a weak separation of scales. Contrary to [Fish et al. \(1994b\)](#), our estimation quantifies the modeling error that occurs on the boundaries thanks to the higher order boundary layer correctors. Indeed, a rapid change of gradients generally occurs near the boundaries, which, ultimately, may be responsible for the failure initiation of the structure ([Pipes et al., 1973](#)). However, it should be noted that the mathematical estimation of such error associated with higher order correctors, though possible based on theorems from mathematical homogenization ([Tartar, 2009](#)), is especially difficult at boundaries and beyond the scope of the present work. The interested reader will find some steps showing the direction towards such mathematical estimation near interfaces in the recent work of [Josien \(2019\)](#).

The adaptivity process generally entails minimizing two types of errors, *viz.* the discretization error, inherent to finite element approximation, and the modeling error, as discussed by [Fish et al. \(1994a\)](#) and [Zohdi et al. \(1996\)](#). To this end, we also study the competition of both discretization and modeling errors for different macroscale

meshes and material phase ratios.

Finally, hierarchical modeling raises the challenge of adequately coupling the macroscale and the microscale domains. Several coupling techniques have been proposed in the literature such as the submodeling technique, which consists in performing two independent analyses, one on the macroscale global model with a coarser mesh, and the other on the microscale local model with a refined mesh (submodel), where the displacement obtained with the global model is prescribed to the boundary of the local one. It will be shown later that this technique generally leads, in the context of multiscale analyses, to high modeling errors on the interfaces. Other coupling techniques that differ according to the physics of the problem exist, such as the volume coupling of Arlequin method (Dhia, 1998), and surface coupling techniques such as the mortar element method (Bernardi et al., 2005; Amini et al., 2009), linear multi-point connection (Lloberas-Valls et al., 2012), or more recently a second-order homogenization based coupling (Wangermez et al., 2020). In this article, we propose a multiscale enhancement of the classical submodeling technique where, instead of applying the macroscale displacement on the local domain, a higher-order localized displacement field corrected at the boundaries is applied. This is expected to give better results since localized fields provide a good estimation of local microscale fields, as will be shown later in this article.

Regarding the aforementioned aspects, the present work proposes the following main novelties:

- A higher-order localization process with boundary layer correction conducted on macroscale coarse meshes to provide an estimation of local microscale fields. A modeling error, based on this estimation, is proposed.
- A multiscale enhanced submodeling technique based on the localized fields

corrected at the boundaries to adequately couple the macroscale with the microscale domains.

To the best of our knowledge, such aspects have not been proposed in the literature yet.

The outline of the paper is as follows. In Sec. 2, we first present the studied boundary value problem and briefly recall the localization process and the boundary layer correction method. In Sec. 3, we detail the proposed procedure to conduct this localization process on coarse macroscale meshes. The suggested modeling error estimation is elaborated in Sec. 4, and the multiscale submodeling technique is depicted in Sec. 5. Each section is accompanied by numerical example to demonstrate the efficiency of the suggested approaches. The analysis is limited to linear elastic material behavior under the small strain assumption.

2. Preliminaries

Asymptotic homogenization can be used to determine the effective properties of periodic materials from the knowledge of local mechanical properties over one unit-cell, representative of the microstructure. This method is also able to estimate, by a localization process, local fields within a structure without conducting DNS. Nevertheless, the solution provided by the localization process is inaccurate in the vicinity of the boundaries due to the loss of periodicity assumption in these regions, unless a boundary layer correction is applied.

In this section, we present the studied boundary value problem and briefly recall the localization procedure and the boundary layer correction method to improve the accuracy of estimated fields on the boundaries. We refer the reader to [Fergoug et al. \(2022a,b\)](#) for more details.

2.1. Statement of the boundary value problem

A heterogeneous periodic body is considered as a linearly elastic solid in static equilibrium, whose heterogeneity arises from the distribution of separate phases at the microscale. We define the bounded domain Ω , shown in Figure 1a, occupied by this heterogeneous body and corresponding to the microscale. The boundary $\partial\Omega$ consists of a portion Γ_u , on which the displacements are prescribed to the value $\mathbf{u}^d = 0$, a portion Γ_t on which a pressure distribution $P(\mathbf{x})$ is applied, and the last portion Γ_s on which the structure is sliding freely. The size of the structure is $L = 12$ mm, $H = 6$ mm, and $W = 1$ mm, with a fiber volume fraction of 25%. The matrix and the inclusions are assumed to be isotropic elastic with coefficients $(E_m = 500$ MPa, $\nu_m = 0.3)$ and $(E_f, \nu_f = 0.3)$, respectively, where the value of E_f will be varied across the examples. This boundary value problem will be solved under the plane strain conditions.

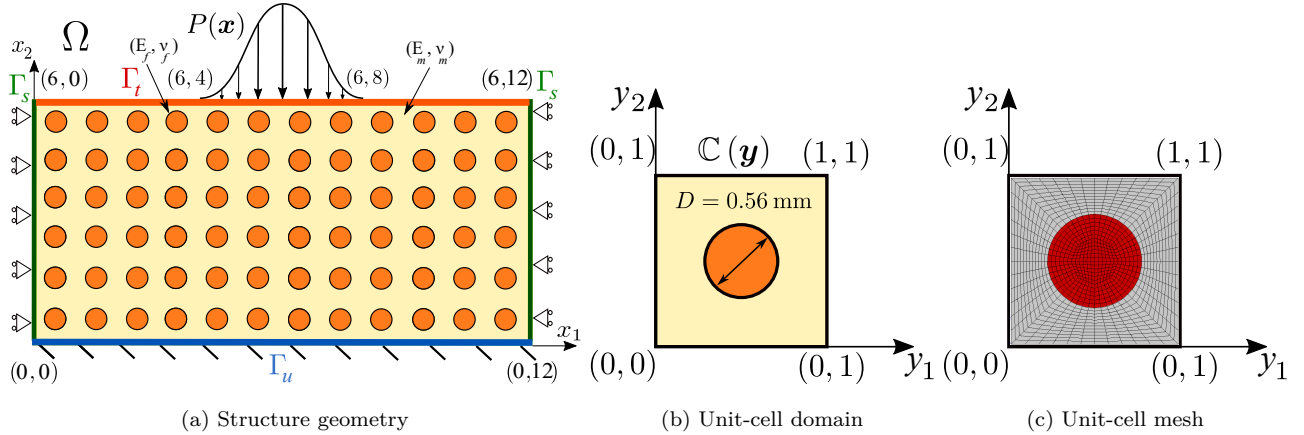


Figure 1: Illustration of the studied fiber-matrix composite. The corresponding microscale mesh is built by repeating the unit-cell Y characterized by a heterogeneous behavior $\mathbb{C}(\mathbf{y})$ over the three space directions. The structure is sliding on Γ_s , fixed on Γ_u and a pressure distribution $P(\mathbf{x})$ is applied on Γ_t .

Due to its heterogeneous nature, the mechanical behavior of the body Ω is assumed to depend on two scales:

- Macroscale with materially homogeneous domain Ω , having L as a characteristic length and global coordinates $\mathbf{x} \in \Omega$, and endowed with homogenized properties $\mathbb{C}^0(\mathbf{x})$, obtained from the resolution of the first-order homogenization problem over the unit-cell;
- Microscale, having l as a characteristic length and with local coordinates $\mathbf{y} \in Y$, where Y is the unit-cell domain, and endowed with heterogeneous properties $\mathbb{C}(\mathbf{y})$.

The coarse and fine scales are related by the parameter ϵ such that:

$$\epsilon = \frac{l}{L}, \quad \mathbf{y} = \frac{\mathbf{x}}{\epsilon}. \quad (1)$$

The finite element mesh describing the unit-cell is composed of 1,008 twenty-node brick elements as shown in Figure 1c. Therefore the microscale mesh describing the entire structure including all heterogeneities is composed of 72,576 ($1,008 \times 6 \times 12$) elements, corresponding to 1,527,345 degrees of freedom.

In Section 2, we consider that the macroscale mesh is identical to the microscale one, but endowed with homogenized properties $\mathbb{C}^0(\mathbf{x})$.

2.2. Localization procedure

In Fergoug et al. (2022b), an estimation of heterogeneous fields has been proposed by conducting a higher-order localization, up to the third-order. The obtained estimates are expected to capture the effect of macroscale successive gradients neglected by a conventional first-order localization. The main aspects of the estimation are

briefly recalled here and the reader is referred to [Fergoug et al. \(2022b\)](#) for more details.

The proposed estimation is constructed by solving the following problems:

- Homogeneous problem (\mathcal{P}_{hom}) with effective behavior $\mathbb{C}^0(\mathbf{x})$. Solving this problem enables to compute the macroscale strain and its successive gradients ($\mathbf{E}(\mathbf{x}), \nabla_{\mathbf{x}}\mathbf{E}(\mathbf{x}), \nabla_{\mathbf{x}}\nabla_{\mathbf{x}}\mathbf{E}(\mathbf{x})$). The gradient of the macroscale strain field, $\nabla_{\mathbf{x}}\mathbf{E}$, is numerically evaluated by extrapolating corresponding strain values between integration points to the nodes and are averaged for each element (at the nodes). Strain values are then appropriately differentiated using the finite element symmetric gradient operator, usually denoted \mathbf{B} . A similar procedure is used to compute the second gradient of the macroscale strain field $\nabla_{\mathbf{x}}\nabla_{\mathbf{x}}\mathbf{E}$.
- First ($\mathcal{P}_{order}^{1st}$), second ($\mathcal{P}_{order}^{2nd}$), and third-order ($\mathcal{P}_{order}^{3rd}$) homogenization problems over the unit-cell. First-, second-, and third-order localization tensors ($\mathbb{D}^0, \mathbb{A}^0, \mathbb{B}^0$), ($\mathbb{D}^1, \mathbb{A}^1, \mathbb{B}^1$), and ($\mathbb{D}^2, \mathbb{A}^2, \mathbb{B}^2$) are obtained from the resolution of these problems, respectively.

The proposed estimates read:

$$\left. \begin{aligned} \mathbf{u}^{est}(\mathbf{x}, \mathbf{y}) &= \mathbf{U}(\mathbf{x}) \\ &+ \epsilon \mathbb{D}^0(\mathbf{y}) : \mathbf{E}(\mathbf{x}) \\ &+ \epsilon^2 \mathbb{D}^1(\mathbf{y}) : \nabla_{\mathbf{x}}\mathbf{E}(\mathbf{x}) \\ &+ \epsilon^3 \mathbb{D}^2(\mathbf{y}) :: \nabla_{\mathbf{x}}\nabla_{\mathbf{x}}\mathbf{E}(\mathbf{x}) \end{aligned} \right\} \forall \mathbf{x} \in \Omega, \forall \mathbf{y} \in Y, \quad (2)$$

$$\left. \begin{aligned} \boldsymbol{\varepsilon}^{est}(\mathbf{x}, \mathbf{y}) &= \mathbb{A}^0(\mathbf{y}) : \mathbf{E}(\mathbf{x}) \\ &+ \epsilon \mathbb{A}^1(\mathbf{y}) : \nabla_{\mathbf{x}} \mathbf{E}(\mathbf{x}) \\ &+ \epsilon^2 \mathbb{A}^2(\mathbf{y}) :: \nabla_{\mathbf{x}} \nabla_{\mathbf{x}} \mathbf{E}(\mathbf{x}) \end{aligned} \right\} \forall \mathbf{x} \in \Omega, \forall \mathbf{y} \in Y, \quad (3)$$

$$\left. \begin{aligned} \boldsymbol{\sigma}^{est}(\mathbf{x}, \mathbf{y}) &= \mathbb{B}^0(\mathbf{y}) : \mathbf{E}(\mathbf{x}) \\ &+ \epsilon \mathbb{B}^1(\mathbf{y}) : \nabla_{\mathbf{x}} \mathbf{E}(\mathbf{x}) \\ &+ \epsilon^2 \mathbb{B}^2(\mathbf{y}) :: \nabla_{\mathbf{x}} \nabla_{\mathbf{x}} \mathbf{E}(\mathbf{x}) \end{aligned} \right\} \forall \mathbf{x} \in \Omega, \forall \mathbf{y} \in Y. \quad (4)$$

Estimated fields in Eqs. 2, 3, 4 are computed using localization tensors combined with the value of the macroscale strain or its gradients *at the current point*, and not its average over the unit-cell (see Figure 2). This localization process improvement, firstly proposed by Kruch and Forest (1998), requires identical microscale and macroscale meshes in order to locate each unit-cell on the macroscale structure (see Figure 2). An extension of this localization process to different coarser macroscale meshes is presented in Section 3. The use of nodal extrapolation on the macroscopic strain field $\nabla_{\mathbf{x}} \mathbf{E}(\mathbf{x})$ in order to compute its successive gradients may induce additional pollution error. Using a higher-order finite element formulation – starting at order three – would be a preferable alternative, but they are seldom available in most finite element softwares and would significantly increase the computational cost of the macroscopic solution. A strain recovery procedure such as the super-convergent one from Zienkiewicz-Zhu Zienkiewicz and Zhu (1992a) is another alternative. However the extrapolation procedure used in this paper does not appear to be the source of much error on the numerical examples, with the advantage of almost no additional cost.

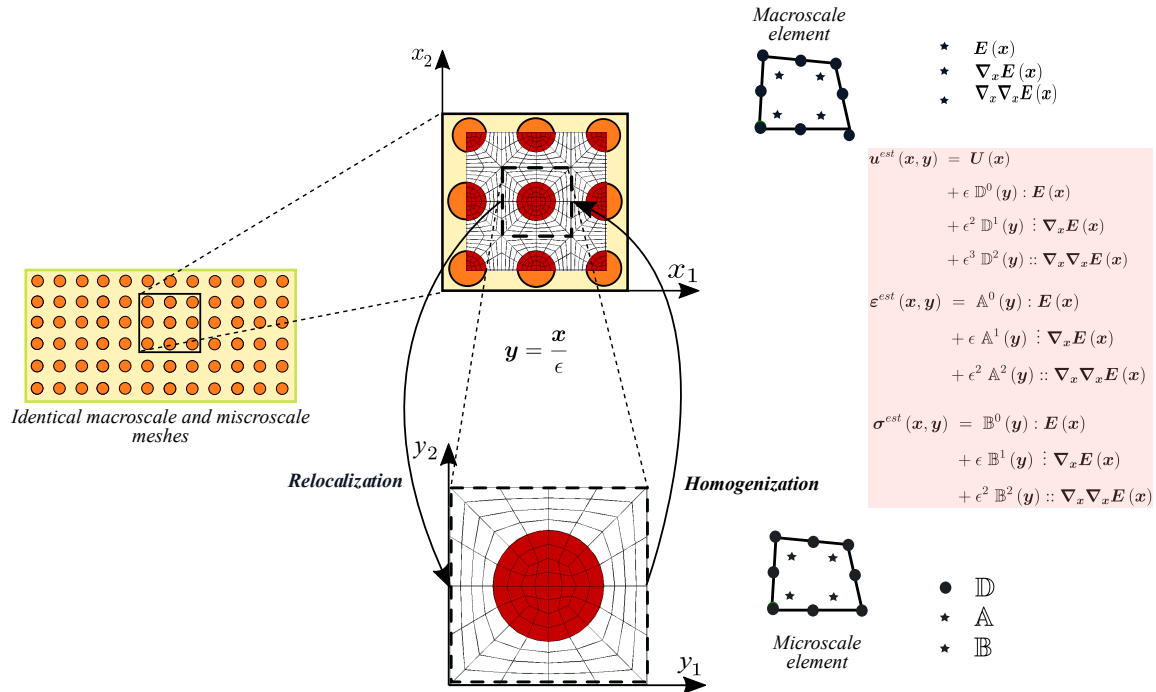


Figure 2: Illustration of the localization procedure. The macroscale strain and its gradients $(\mathbf{E}(\mathbf{x}), \nabla_{\mathbf{x}} \mathbf{E}(\mathbf{x}), \nabla_{\mathbf{x}} \nabla_{\mathbf{x}} \mathbf{E}(\mathbf{x}))$ are stored at the integration points of the macroscale elements. Strain and stress localization tensors (\mathbb{A}, \mathbb{B}) are stored at the integration points of the microscale elements of the unit-cell, and the displacement localization tensor \mathbb{D} on the nodes. Estimated fields are computed after locating the unit-cell mesh on the macroscale one.

2.3. Boundary layer correction

Homogenization procedures are generally unable to provide an accurate estimation of local fields near the boundaries. Indeed, a complex stress (or strain) field occurs within a very local region near the boundaries, frequently referred to as a *boundary layer effect*. Following previous work of Dumontet (1986), we have proposed a general method to correct higher-order estimates on the boundaries, valid for various Boundary Conditions (BCs): Dirichlet, Neumann, or mixed. The main idea of the correction is summarized, for Dirichlet BCs, in Figure 3. The localization pro-

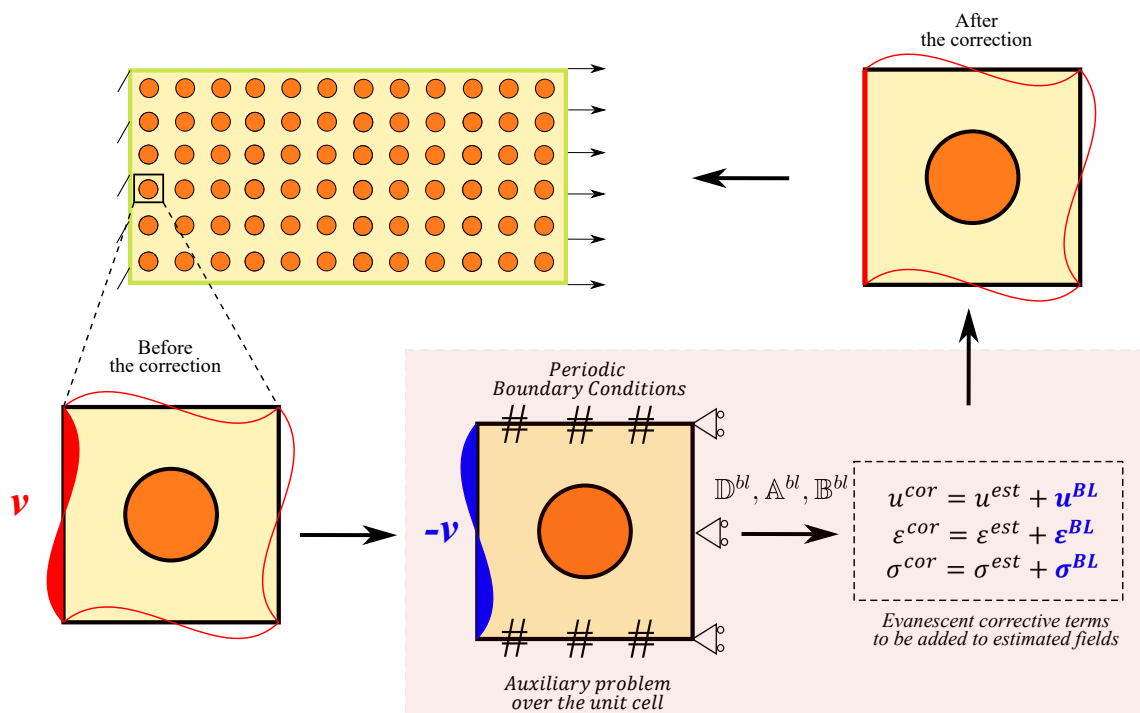


Figure 3: Illustration of the boundary layer correction method for a Dirichlet boundary. Localization processes provide a spurious periodic fluctuation \mathbf{v} on the boundary. The inverse of this fluctuation is applied to an auxiliary problem over the unit-cell, providing boundary layer displacement, strain, and stress localization tensors. After a localization process on the concerned boundary, evanescent corrective terms are computed and added to estimated fields.

cess provides a spurious periodic fluctuation \mathbf{v} on the boundary. The opposite of this fluctuation is applied to an auxiliary problem subjected to adequate periodic boundary conditions. Solving this problem enables to obtain first, second, or third-order boundary layer displacement, strain, and stress localization tensors $(\mathbb{D}^{0,bl}, \mathbb{A}^{0,bl}, \mathbb{B}^{0,bl})$, $(\mathbb{D}^{1,bl}, \mathbb{A}^{1,bl}, \mathbb{B}^{1,bl})$, and $(\mathbb{D}^{2,bl}, \mathbb{A}^{2,bl}, \mathbb{B}^{2,bl})$, respectively. Afterward, boundary layer correctors $(\mathbf{u}^{bl}, \boldsymbol{\epsilon}^{bl}, \boldsymbol{\sigma}^{bl})$ are computed by conducting similar localization processes, detailed in Figure 2, on the concerned boundary.

Remark 1. A particular treatment was considered for boundary layer correction of

corner cells, as explained by [Fergoug et al. \(2022a\)](#).

In what follows, we consider the following fields:

- Microscale fields obtained by solving problem (\mathcal{P}_{ref}) using DNS, which will be considered as our reference, indexed *ref*, with solution $(\mathbf{u}^{ref}, \boldsymbol{\varepsilon}^{ref}, \boldsymbol{\sigma}^{ref})$.
- Homogeneous fields obtained by solving problem (\mathcal{P}_{hom}), indexed *hom*, with solution (displacement \mathbf{U} , strain \mathbf{E} , stress $\boldsymbol{\Sigma}$).
- Proposed first-, second-, and third-order estimates of microscale fields obtained by the first-, second-, and third-order localization processes, indexed *est1*, *est2*, and *est3*, respectively.
- Proposed first-, second-, and third-order boundary layer corrections of estimated fields indexed *cor1*, *cor2*, and *cor3*, respectively.

3. Extension of the localization procedure to arbitrary macroscale meshes

Asymptotic homogenization enables, by a localization process, to estimate the microscale fields from the knowledge of the formerly determined macroscale fields. In this section, we propose an extension of the localization process described in Section 2, to deal with *coarser* macroscale meshes. As a result, global balance and microscale fields are estimated on the macroscale mesh, requiring much less computational cost than DNS.

3.1. Proposed localization technique

The localization process is illustrated in Figure 4. A cell box, with the same dimensions of the unit-cell mesh, is being moved around the global mesh. Integration Points (IPs) of the macroscale elements inside the moving box are then selected.

For each of these macroscale IPs, its nearest microscale IP is then identified after mapping the unit-cell on the current position of the moving box. A first localization step is conducted over the global mesh by contracting the strain field (or its gradients) values of the current macroscale IP with localization tensors of the identified nearest microscale IP. Afterward, the localized field is corrected at the boundaries by using the same previously described approach on the concerned boundary. Instead of evaluating gradients on average, on macroscopic regions corresponding to a unit-cell, we choose to evaluate them at macroscopic IPs. This does not stem from an exact mathematical motivation but from necessity due to the absence of full separation of scales. This point is rarely discussed in the literature. Nevertheless, the two approaches have been compared by [Kruch and Forest \(1998\)](#) and a clear advantage has been empirically demonstrated for the evaluation at macroscopic IPs. This approach has also been successfully applied by other authors [Feyel and Chaboche \(2001\)](#); [Yvonnet and Bonnet \(2014\)](#); [He and Pindera \(2020\)](#).

The higher-order stress localization process is detailed in Algorithm 1 (the same procedure is used for strain localization). To conduct the displacement localization process, the displacement localization tensor \mathbb{D} , originally stored at the nodes of the unit-cell mesh, is interpolated to integration points. Therefore, the localization process can be carried out as previously discussed. The obtained result, which is a displacement correction on the macroscale mesh, is then extrapolated to nodes and added to the macroscale displacement field, as shown for \mathbf{u}^{est} in Figure 2.

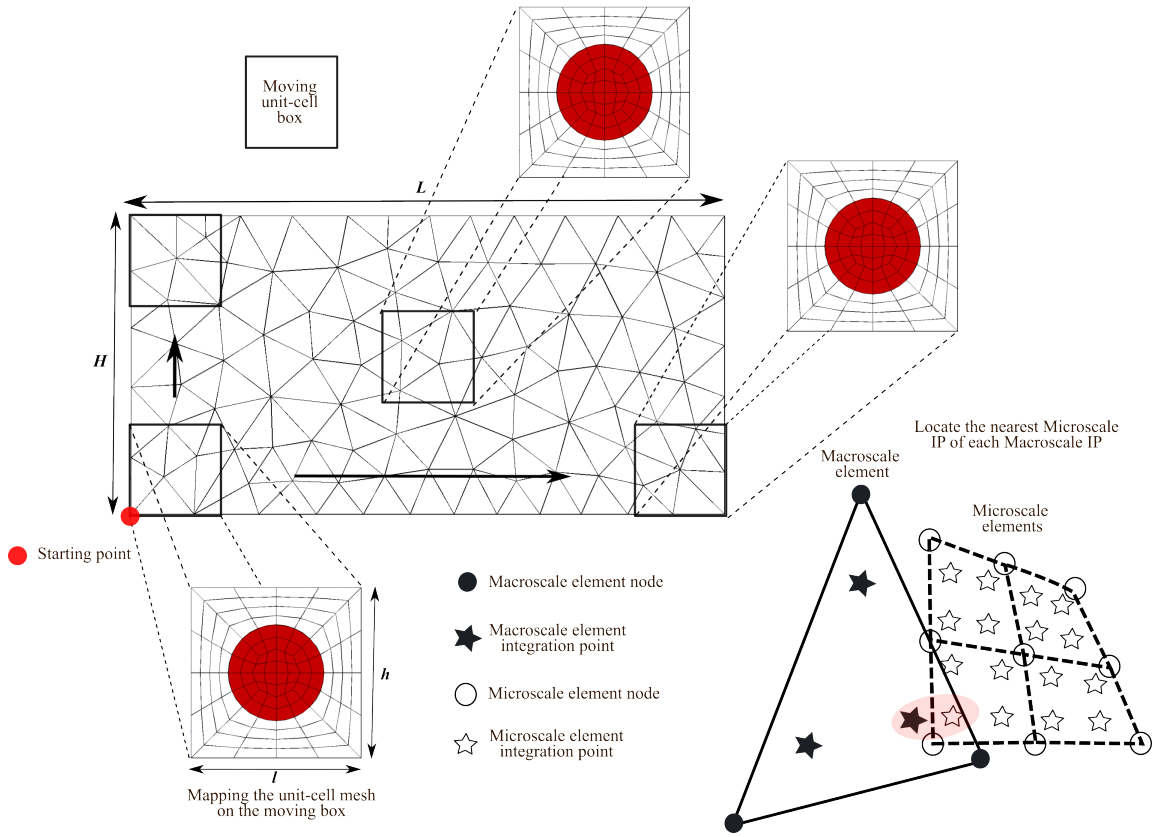


Figure 4: Illustration of the localization process on a coarser macroscale mesh.

3.2. Numerical results

To illustrate the effectiveness of the proposed localization process, six macroscale unstructured meshes composed of fifteen-node wedge elements are considered, as shown in Figure 5. The ratio between the numbers of microscale and macroscale degrees of freedom varies from 560 for the coarsest mesh (see Figure 5a) to 2 for the finest one (see Figure 5f). A mesh adaptation technique, with a target elements size obtained through the a posteriori discretization error estimator ZZ2 (Zienkiewicz and Zhu, 1992a,b), is used to generate macroscale meshes (see Figures 5c, 5d, 5e, 5f) refined in areas of interest, where stress concentrations occur. For the finest macroscale mesh, the mesh adaptation procedure has been performed while preserving the topology of the fibers (see Figure 5f). For this example, we consider a ratio $\frac{E_f}{E_m} = 10$ and a localization process with boundary layer correction up to the second-order, as it is sufficient to capture strain gradients in the present example.

A comparison of σ_{22} and σ_{12} is shown in Figures 6 and 7, respectively (other stress and displacement components are presented in Appendix A). By comparing reference fields, σ_{22}^{ref} and σ_{12}^{ref} , with localized fields, one can notice that the quality of the predicted stresses increases by refining the macroscale mesh. Nevertheless, the contribution of different material phase (matrix and fibers) to the stress field becomes visible starting from macroscale mesh 3, which provides an acceptable estimation of reference fields even though it contains 113 times fewer degrees of freedom than the microscale problem. Furthermore, high stress gradients, especially near regions where the load is applied and on the interfaces, are correctly predicted starting from macroscale mesh 3.

This localization process provides valuable insights on local responses of the constituents, at any material point, for a given macroscale state computed on a coarse mesh, which is significantly less computationally expensive than DNS. This is of spe-

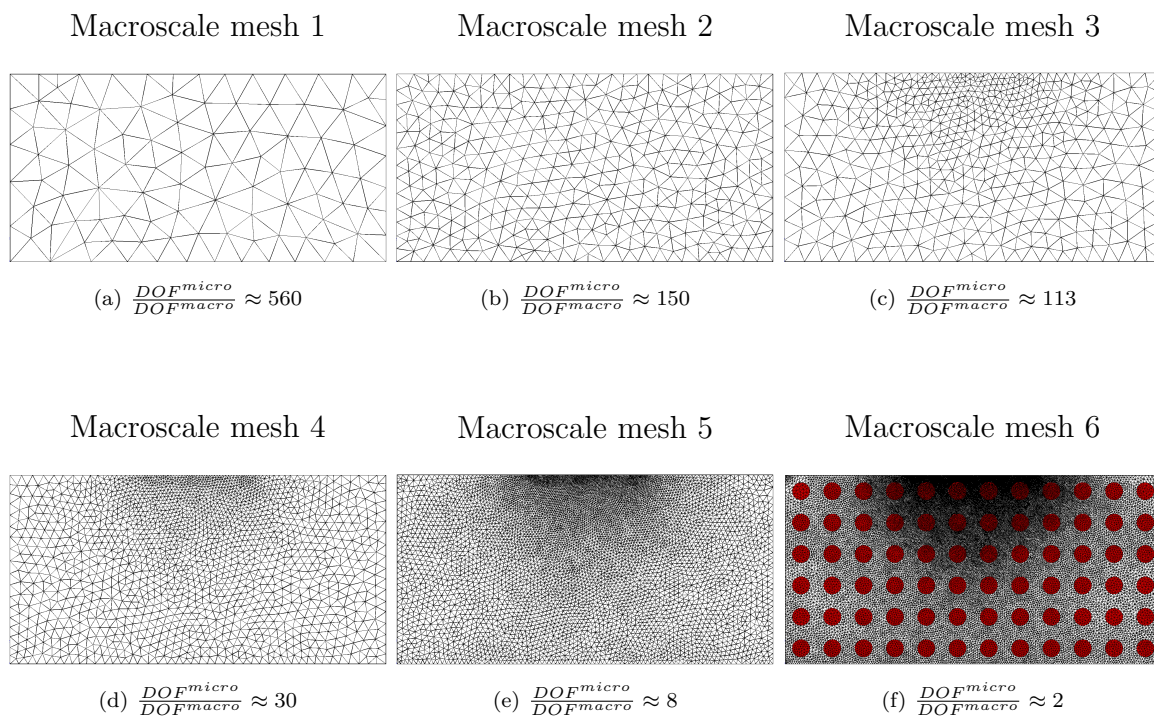
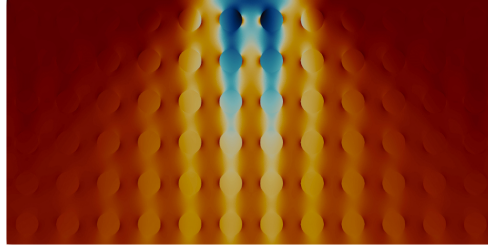


Figure 5: Macro-scale meshes on which the global balance and localization processes are performed.

cial interest for identifying local deformation mechanisms and quantities of interest such as damage. Furthermore, estimating local fields on macro-scale meshes is a path toward error estimation and efficient multiscale submodeling, as it will be shown in the next sections.

4. Modeling error: A bridge between scales

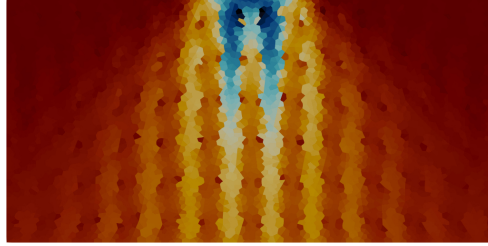
Solving DNS is generally intractable because of the resulting extremely fine spatial discretization mesh. Nevertheless, there is a need to investigate what could occur at the microscale, since the behavior of heterogeneous structures depends on the characteristics of the heterogeneities. One method to tackle this is to *adaptively* couple a fine heterogeneous material description in some regions of the domain and a



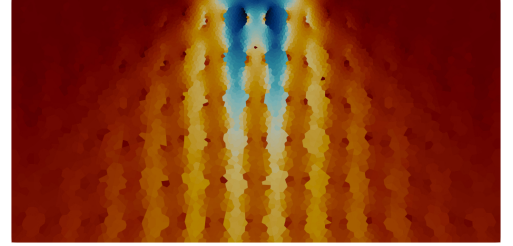
(a) σ_{22}^{ref} on microscale mesh



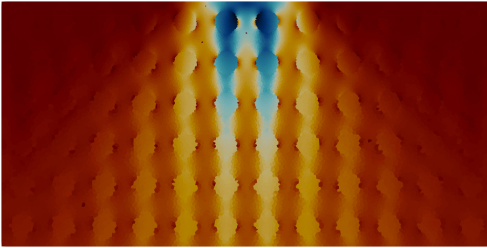
(b) σ_{22}^{cor2} on macroscale mesh 1



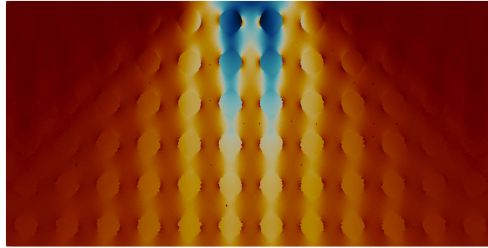
(c) σ_{22}^{cor2} on macroscale mesh 2



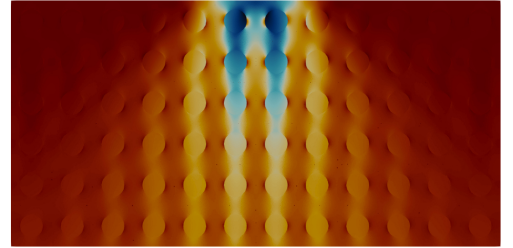
(d) σ_{22}^{cor2} on macroscale mesh 3



(e) σ_{22}^{cor2} on macroscale mesh 4



(f) σ_{22}^{cor2} on macroscale mesh 5



(g) σ_{22}^{cor2} on macroscale mesh 6

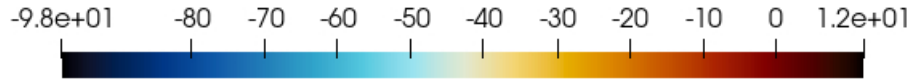
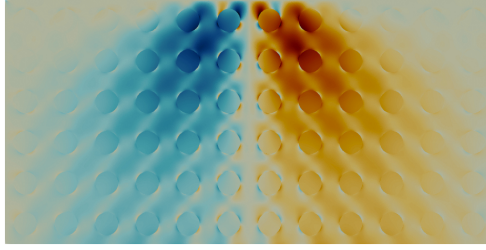


Figure 6: Comparison of σ_{22} (MPa) results.

coarse, less accurate macroscale model in the other regions. For this purpose, one can use the well known submodeling techniques, which will be investigated in Section 5. In this work, a modeling error is used to steer this adaptive modeling process by detecting areas where refining the material model is required.



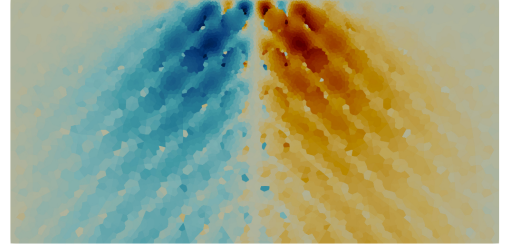
(a) σ_{12}^{ref} on microscale mesh



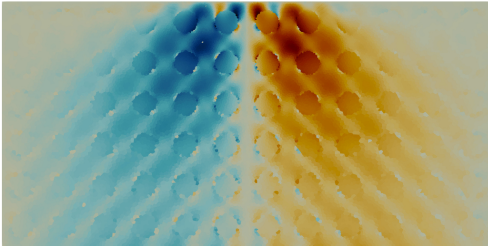
(b) σ_{12}^{cor2} on macroscale mesh 1



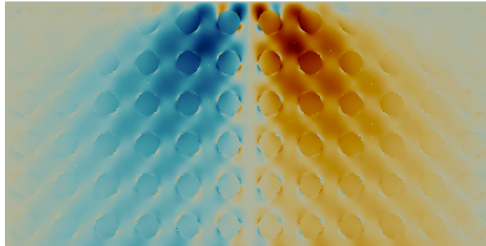
(c) σ_{12}^{cor2} on macroscale mesh 2



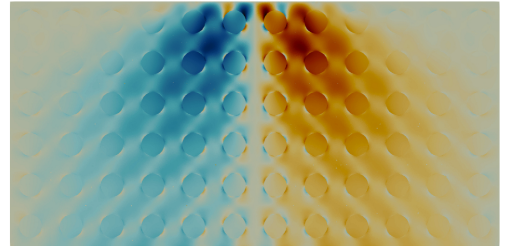
(d) σ_{12}^{cor2} on macroscale mesh 3



(e) σ_{12}^{cor2} on macroscale mesh 4



(f) σ_{12}^{cor2} on macroscale mesh 5



(g) σ_{12}^{cor2} on macroscale mesh 6



Figure 7: Comparison of σ_{12} (MPa) results.

4.1. Formulation of the modeling error estimator

We recall that \mathbf{u}^{ref} , solution to (\mathcal{P}_{ref}) , is the reference displacement field computed by DNS. This field can be approximated with an asymptotic expansion in

powers of the small parameter ϵ as:

$$\mathbf{u}^{ref}(\mathbf{x}) = \underbrace{\mathbf{u}^0(\mathbf{x}, \mathbf{y}) + \epsilon \mathbf{u}^1(\mathbf{x}, \mathbf{y})}_{\mathbf{u}^{est1}} + \underbrace{\epsilon^2 \mathbf{u}^2(\mathbf{x}, \mathbf{y})}_{\mathbf{u}^{est2}} + \underbrace{\epsilon^3 \mathbf{u}^3(\mathbf{x}, \mathbf{y}) + \dots}_{\mathbf{u}^{est3}}, \quad (5)$$

where the quantities \mathbf{u}^n are Y -periodic functions called *correctors* of the displacement field. The first-, second-, and third-order localized displacement fields, \mathbf{u}^{est1} , \mathbf{u}^{est2} , and \mathbf{u}^{est3} , are obtained by truncating the asymptotic expansion to the first-, second-, and third-order, respectively (see Equation 5).

As stated before, estimated fields are generally incorrect in the vicinity of the boundaries due to the loss of periodicity in these regions. Indeed, matching boundary conditions requires the introduction of boundary layer correctors at each localization order. As a result of this correction, \mathbf{u}^{cor1} , \mathbf{u}^{cor2} , and \mathbf{u}^{cor3} are the first-, second-, and third-order corrected fields on the boundaries, respectively (see Algorithm 1).

For the purpose of the following developments, we define the measure of the local (element-wise) *true* modeling error in L^2 norm as :

$$\left\| \mathbf{u}^{ref} - \mathbf{u}^{est1} \right\|_{L_2(\Omega_e)} = \left(\int_{\Omega_e} (\mathbf{u}^{ref} - \mathbf{u}^{est1}) \cdot (\mathbf{u}^{ref} - \mathbf{u}^{est1}) d\Omega_e \right)^{\frac{1}{2}}, \quad (6)$$

and the corresponding measure in energy norm as :

$$\left\| \mathbf{u}^{cor3} - \mathbf{u}^{est1} \right\|_{E(\Omega_e)} = \left(\int_{\Omega_e} (\boldsymbol{\epsilon}^{cor3} - \boldsymbol{\epsilon}^{est1}) : (\boldsymbol{\sigma}^{cor3} - \boldsymbol{\sigma}^{est1}) d\Omega_e \right)^{\frac{1}{2}}, \quad (7)$$

where Ω_e denotes the domain of an element. The corresponding global true modeling error $\left\| \mathbf{u}^{ref} - \mathbf{u}^{est1} \right\|_{\bullet(\Omega)}$, for both norms, reads:

$$\left\| \mathbf{u}^{ref} - \mathbf{u}^{est1} \right\|_{\bullet(\Omega)}^2 = \sum_e \left\| \mathbf{u}^{ref} - \mathbf{u}^{est1} \right\|_{\bullet(\Omega_e)}^2, \quad (8)$$

where Ω denotes the structural domain area and \bullet stands for L^2 or E .

For this study, the reference problem *is* tractable by Direct Numerical Simulation (DNS) and its mechanical fields are used as reference results to validate our approach. However, in the more general case where a DNS would be out of reach, common practice would call for a tractable estimate.

Consequently, we choose to estimate the modeling error by replacing \mathbf{u}^{ref} with the best estimate of the displacement field yet, *i.e.* \mathbf{u}^{cor3} . The modeling error is then estimated by:

$$\left\| \mathbf{u}^{ref} - \mathbf{u}^{est1} \right\|_{\bullet,(\Omega)} \approx \left\| \mathbf{u}^{cor3} - \mathbf{u}^{est1} \right\|_{\bullet,(\Omega)}. \quad (9)$$

The proposed modeling error estimator quantifies the terms neglected by a first-order localization. These terms are generally negligible in the case of a complete separation of scales. Nevertheless, for weak separation of scales, these terms become significant and necessary to capture gradients of the macroscale field. The proposed estimation also quantifies the modeling error that occurs on the boundaries.

From a different perspective, since the macroscopic behavior remains a simple Cauchy medium, all higher order localisation terms and all the boundary corrector terms act as additional energy contributions that *do not* respect the Hill-Mandel lemma. Therefore, the error estimator built on the basis of these contributions may also be considered an Hill-Mandel energy error.

Remark 2. *The modeling error estimation can be formulated using other mechanical fields than the displacement in conjunction with the L^2 norm, *i.e.* the strain, or the stress field ($\|\boldsymbol{\varepsilon}^{cor3} - \boldsymbol{\varepsilon}^{est1}\|_{L_2(\Omega)} = (\int_{\Omega} (\boldsymbol{\varepsilon}^{cor3} - \boldsymbol{\varepsilon}^{est1}) : (\boldsymbol{\varepsilon}^{cor3} - \boldsymbol{\varepsilon}^{est1}) d\Omega)^{\frac{1}{2}}$ and $\|\boldsymbol{\sigma}^{cor3} - \boldsymbol{\sigma}^{est1}\|_{L_2(\Omega)}$, respectively).*

4.2. Comparison with the discretization error

In general, localized solutions, \mathbf{u}^{cor3} and \mathbf{u}^{est1} , are obtained by a finite dimensional approximation, which is, in our case, a finite element approximation $\mathbf{u}^{cor3,h}$ and

$\mathbf{u}^{est1,h}$, obtained on the macroscale mesh. By the triangle inequality, one can obtain:

$$\begin{aligned} \|\mathbf{u}^{cor3} - \mathbf{u}^{est1}\|_{\bullet(\Omega)} &\leq \underbrace{\|\mathbf{u}^{est1} - \mathbf{u}^{est1,h}\|_{\bullet(\Omega)} + \|\mathbf{u}^{cor3} - \mathbf{u}^{cor3,h}\|_{\bullet(\Omega)}}_{\text{Discretization error: } \eta_{disc}} \\ &\quad + \underbrace{\|\mathbf{u}^{cor3,h} - \mathbf{u}^{est1,h}\|_{\bullet(\Omega)}}_{\text{Modeling error: } \eta_{mod}}. \end{aligned} \quad (10)$$

Therefore, a bipartite discretization error, indexed η_{disc} , occurs. The first and second parts constituting this error are due to the numerical approximation of \mathbf{u}^{est1} and \mathbf{u}^{cor3} , respectively. As this study is mainly devoted to the modeling error estimation, in order to estimate the *true* discretization error in a simple but accurate way, we shall consider that the reference solutions of \mathbf{u}^{est1} and \mathbf{u}^{cor3} are obtained by conducting the localization process and boundary layer correction on the fine microscale mesh (see Figure 8). Therefore, an interpolation-based nodal field transfer of $\mathbf{u}^{est1,h}$ and $\mathbf{u}^{cor3,h}$ from the macroscale mesh to the microscale one is considered (see Figure 8) in order to compute the two terms involved in η_{disc} . This nodal transfer preserves the continuum fields with no information loss since the coarse finite element space is included in the fine one (Dureisseix and Bavestrello, 2006). This allows us to compute an accurate estimation of the discretization error, but is limited to a measure in the L^2 norm. On the other hand, the modeling error estimation, indexed η_{mod} , is computed on the macroscale mesh (see Figure 8) in both L^2 and energy norm. Finally, we also introduce the relative global discretization (resp. modeling) error $\eta_{disc,rel}$ (resp. $\eta_{mod,rel}$) as:

$$\eta_{disc,rel} = \frac{\eta_{disc}}{\|\mathbf{u}^{ref}\|_{\bullet(\Omega^{sub})}}, \quad \eta_{mod,rel} = \frac{\eta_{mod}}{\|\mathbf{u}^{ref}\|_{\bullet(\Omega^{sub})}}. \quad (11)$$

Remark 3. *As the measure in the energy norm involves gradients of the displacement solution, which are defined at integration points and, thus, does not belong to*

a functional space, applying the previous approach to compute the energy norm of the discretization error estimate would imply to resort to integration point based field transfer, such as nearest Gauss points, on $\varepsilon^{est1,h}$, $\varepsilon^{cor3,h}$, $\sigma^{est1,h}$ and $\sigma^{cor3,h}$. This would induce additional pollution error that may degrade the accuracy of the discretization error estimate. Consequently, only the modeling error estimation will be studied in both L^2 and energy norm.

Remark 4. On real use cases, localization procedure on the microscale mesh is computationally intractable. In this case one can use well known a posteriori error estimators, which enables to estimate the discretization error in energy norm, such as the ZZ2 discretization error estimator (Zienkiewicz and Zhu, 1992a,b).

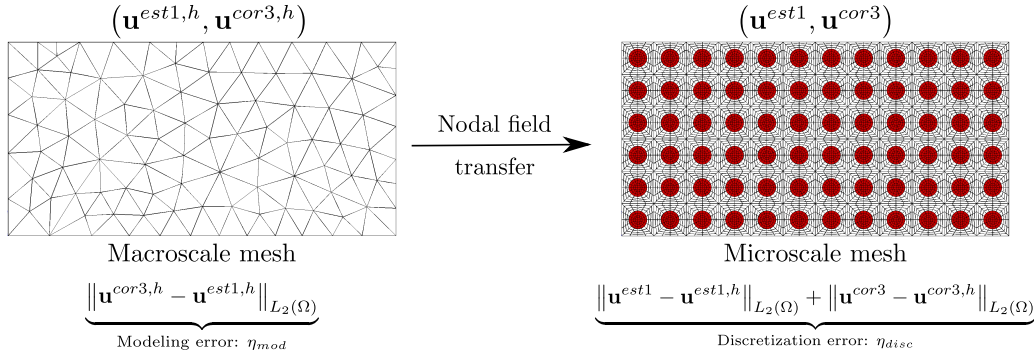


Figure 8: Illustration of the error estimation process. The modeling error is computed on the macroscale mesh. A nodal field transfer of $\mathbf{u}^{est1,h}$ and $\mathbf{u}^{cor3,h}$ to the microscale mesh is conducted to compute the discretization error.

4.3. Numerical results

Relative point-wise contributions to modeling and discretization errors, for a ratio $\frac{E_f}{E_m} = 10$ and $\frac{E_f}{E_m} = 500$, are shown in Figures 9 and 10, respectively. The

localization process with boundary layer correction is considered up to the second-order, as it is sufficient to capture strain gradient effects since the second gradient of the macroscale field was found to be negligible in this case. A comparison of the reference solution \mathbf{u}^{ref} , with the obtained localized fields, \mathbf{u}^{est1} and \mathbf{u}^{cor2} , is shown in Appendix B.

Both parts of the discretization error decrease by refining the macroscale mesh and start to cluster mainly on the fiber/matrix interfaces starting at mesh 4, until mesh 6 which preserves the topology of the fibers and, therefore, preserves the interfaces (see Figure 5f). One can notice that the second part of the discretization error, related to \mathbf{u}^{cor2} , is slightly higher than the first part due to numerical errors emanating from the computation of second-order localization and boundary layer correctors. The modeling error, contrarily to the discretization error, varies only a little bit by refining the macroscale mesh.

Global relative discretization error, $\eta_{disc,rel}$, and relative modeling error, $\eta_{mod,rel}$, in L^2 norm for different ratios $\frac{E_f}{E_m}$ are shown in Figure 11. Global relative modeling error η_{mod} in energy norm is also plotted in Figure 12a. Global values of the discretization error decrease by refining the macroscale mesh, whereas modeling error remains relatively constant whatever the norm used.

The modeling (and discretization) error estimation is relatively independent of the mismatch ratio $\frac{E_f}{E_m}$, especially for ratios higher than 50, as shown in Figure 11 and 12a. This low contrast dependency is a key difference with the modeling error estimator proposed by Zohdi et al. (1996), which highly depends on the material phase contrast. This is explained by the fact that their estimator quantifies the error emanated from the difference between the heterogeneous and the homogeneous materials, which can be high for important contrast ratios. Contrarily, our proposed modeling error estimator is constructed based on the quality of the approximation

of heterogeneous fields, explaining the low contrast dependency, a property desirable in a modeling error estimator.

In order to measure the quality of our proposed modeling error estimator, we introduce the associated effectivity index ζ_{mod} as:

$$\zeta_{mod} = \frac{\eta_{mod}}{\eta_{mod,ref}}, \quad \text{with} \quad \eta_{mod,ref} = \left\| \mathbf{u}^{ref} - \mathbf{u}^{est1} \right\|_{E(\Omega)}. \quad (12)$$

$\eta_{mod,ref}$ stands for the approximation of the *true* modeling error, computed from the DNS solution \mathbf{u}^{ref} and the first-order relocalized solution \mathbf{u}^{est1} of the homogenized problem (\mathcal{P}_{hom}) on the fine microscale mesh. Both quantities involved in η_{mod} (resp. $\eta_{mod,ref}$) are defined on the same macroscale (resp. microscale) mesh, avoiding the use of field transfer procedure and thus extra numerical pollution. Figure 12b shows the evolution of ζ_{mod} for all the macroscale meshes and different ratios $\frac{E_f}{E_m}$. On the problem studied, the proposed modeling error estimator in energy norm gives an upper bound of the modeling error. Besides, the values tend to be independent of the ratio $\frac{E_f}{E_m}$ and quickly stabilize when the discretization error reach the same order of magnitude than the modeling one.

Also, regarding the competition between the discretization and the modeling error illustrated in Figure 11, one shall consider a mesh refinement procedure to reduce the discretization error, and this until a refinement degree between mesh 3 and mesh 4 where the modeling error becomes dominant. One way to reduce this modeling error is to conduct an adaptive modeling process. This is analogous to mesh refinement, except that the refinement is in terms of the material model, *i.e.* replacing a homogeneous material by a heterogeneous one in regions with high modeling error.

5. Multiscale submodeling

The relative modeling error estimation of the stress field, *i.e.*

$$\frac{\|\boldsymbol{\sigma}^{cor2} - \boldsymbol{\sigma}^{est1}\|_{L_2(\Omega_e)}}{\|\boldsymbol{\sigma}^{ref}\|_{L_2(\Omega)}}, \quad (13)$$

on macroscale mesh 3 and for a ratio $\frac{E_f}{E_m} = 500$ is illustrated in Figure 13. To reduce this error, one can replace the homogeneous material by the heterogeneous material in regions where the modeling error is relatively high. These regions to be replaced depend on target accuracy, as suggested in Figure 13. Indeed, replacing the microscale region labeled *submodel 3* is expected to reduce the modeling error more than inserting *submodel 2*, which itself will reduce the error more than inserting *submodel 1*.

For hierarchical modeling, it is necessary to adequately couple the macroscale homogeneous domain with the selected microscale heterogeneous one. Such coupling is proposed in this section.

5.1. Proposed coupling strategy

Submodeling, also called structural zoom or global-local analysis, is largely used in the industry to conduct multiscale analyses since it is supported by most commercial finite element software (*e.g.* Abaqus or Ansys). In this approach, homogenized material properties are first determined, in our case using asymptotic homogenization. The macroscale problem is then solved using these homogeneous properties. The displacements are extracted from the boundary of a macroscale region of interest (Γ_G in Figure 14). These fields become the boundary conditions (on Γ_L in Figure 14) for a finite element *submodel* that contains microscale details, as shown in Figure 14.

Remark 5. *Using displacement field interpolation, the submodel boundary Γ_L nodes do not have to match with the macroscale boundary Γ_G nodes.*

Classical submodeling, *i.e.* applying \mathbf{u}^0 , is expected to fail in appropriately coupling the macroscale with the microscale, and this no matter the size of the submodel, as it will be shown later, for the following reasons:

- The homogenized displacement \mathbf{u}^0 , misses, by definition, the microscale details. The coupling, therefore, neglects the heterogeneous nature of the submodel, which result in high interface coupling errors. Consequently, it is necessary to enlarge the submodel to avoid coupling errors in a region of interest as shown in Figure 15, which can be computationally expensive.
- Homogeneous fields are only valid for infinite periodic arrays under a uniform state of macro-stress (or macro-strain). This is not the case for weak separation of scale scenarios.
- Homogenized solutions do not take into account the boundary layer effect due to the loss of periodicity conditions on the boundaries.

In what follows, the proposed submodeling is performed by applying \mathbf{u}^{cor2} instead of \mathbf{u}^{cor3} , since the second gradient of the macroscale field was found to be negligible in this case.

The proposed submodeling considers the aforementioned aspects since the displacement field \mathbf{u}^{cor2} is heterogeneous by construction, takes into account macroscale strain gradients, and is corrected at the boundaries.

It is worth noting that the submodeling approach is a *descending* process in the sense that there is no feedback from the submodel computation toward the macroscale one.

Such feedback is necessary to conduct reliable hierarchical modeling. However, this aspect is left for future works.

5.2. Numerical results

To compare the reference solution \mathbf{u}^{ref} with the displacement field obtained using classical submodeling $\mathbf{u}^{\mathcal{L}}$ or the proposed submodeling $\mathbf{u}^{\mathcal{L}^*}$, the following local (element-wise) error in energy norm is defined:

$$\begin{aligned} \|\mathbf{e}\|_{E(\Omega_e)} &= \|\mathbf{u}^{ref} - \mathbf{u}^k\|_{E(\Omega_e)} \\ &= \left(\int_{\Omega_e} (\boldsymbol{\varepsilon}^{ref} - \boldsymbol{\varepsilon}^k) : (\boldsymbol{\sigma}^{ref} - \boldsymbol{\sigma}^k) d\Omega_e \right)^{\frac{1}{2}}, \end{aligned} \quad (14)$$

where Ω_e denotes the domain of an element and $k = (\mathcal{L} \text{ or } \mathcal{L}^*)$. Thus, the global error $\|\mathbf{e}\|_{E(\Omega^{sub})}$ on the submodel reads:

$$\|\mathbf{e}\|_{E(\Omega^{sub})}^2 = \sum_e \|\mathbf{e}\|_{E(\Omega_e^{sub})}^2, \quad (15)$$

and its relative counterpart e_{rel} reads:

$$e_{rel} = \frac{\|\mathbf{e}\|_{E(\Omega^{sub})}^2}{\|\mathbf{u}^{ref}\|_{E(\Omega^{sub})}^2}, \quad (16)$$

where Ω^{sub} denotes the domain of the chosen submodel. We define the local (element-wise) relative error as:

$$e_{rel,e} = \frac{\|\mathbf{e}\|_{E(\Omega_e)}^2}{\|\mathbf{u}^{ref}\|_{E(\Omega^{sub})}^2}. \quad (17)$$

We also consider a quantity of interest e^{mean} , corresponding to the mean error in the region of interest Ω^{sub1} illustrated in Figure 14:

$$e^{mean} = \frac{1}{|\Omega^{sub1}|} \left[\sum_e \|\mathbf{e}\|_{E(\Omega_e^{sub1})}^2 \right]^{1/2}, \quad (18)$$

and its relative counterpart e_{rel}^{mean} defined as:

$$e_{rel}^{mean} = \frac{e^{mean}}{u^{mean}}, \quad (19)$$

with:

$$u^{mean} = \frac{1}{|\Omega^{sub1}|} \left[\sum_e \left\| \mathbf{u}^{ref} \right\|_{E(\Omega_e^{sub1})}^2 \right]^{1/2}. \quad (20)$$

Figure 15 shows a comparison of the relative error, defined in Equation 17, obtained by using the classical submodeling ($k = \mathcal{L}$) and the proposed one ($k = \mathcal{L}^*$), for the three submodels illustrated in Figure 13, and for ratio $\frac{E_f}{E_m} = 500$. The macromesh 3, shown in Figure 5c, is used for the macroscale computation and the localization process. The relative error is drastically reduced by the proposed submodeling compared to the classical one, for the three submodels and the considered ratios. Indeed, classical submodeling leads to large errors, especially in the vicinity of the coupling interfaces. This coupling error increases by increasing the material phase contrast. The proposed submodeling enables to reduce the mean error e_{rel}^{mean} by a factor of ≈ 5 for submodel 1 and a factor of ≈ 3 for submodels 2 and 3.

Comparison of the global relative error e_{rel} , formulated in Equation 16, obtained by using the classical and the proposed submodeling, is shown in Table 1, where the macromesh 3 is also used for the macroscale computation and the localization process. One can notice that the global error increases by increasing the material phase contrast. The proposed coupling reduces the global error by a factor of ≈ 5 for submodel 1, a factor of ≈ 3 for submodel 2 and a factor of ≈ 4 for submodel 3.

To study the influence of the macroscale mesh on the proposed submodeling, a comparative study is presented in Figure 16, investigating the relative error and the mean error obtained for a coupling with different macroscale meshes, illustrated in Figure 5, and for different submodels, shown in Figure 13. The material phase contrast considered in this study is $\frac{E_f}{E_m} = 500$.

Table 1: Comparison of the global relative error e_{rel} defined in Equation 16, obtained by using the classical *vs* the proposed submodeling. The macromesh 3 (illustrated in Figure 5c) is used for the macroscale computation and the localization process.

Ratio / Submodel	1		2		3	
	Classical	Proposed	Classical	Proposed	Classical	Proposed
10	8.50%	<i>vs</i> 1.74%	7.03%	<i>vs</i> 2.11%	10.79%	<i>vs</i> 2.90%
50	9.91%	<i>vs</i> 2.06%	8.18%	<i>vs</i> 2.51%	12.53%	<i>vs</i> 3.41%
100	10.11%	<i>vs</i> 2.04%	8.33%	<i>vs</i> 2.54%	12.77%	<i>vs</i> 3.46%
500	10.26%	<i>vs</i> 2.06%	8.46%	<i>vs</i> 2.56%	12.96%	<i>vs</i> 3.50%

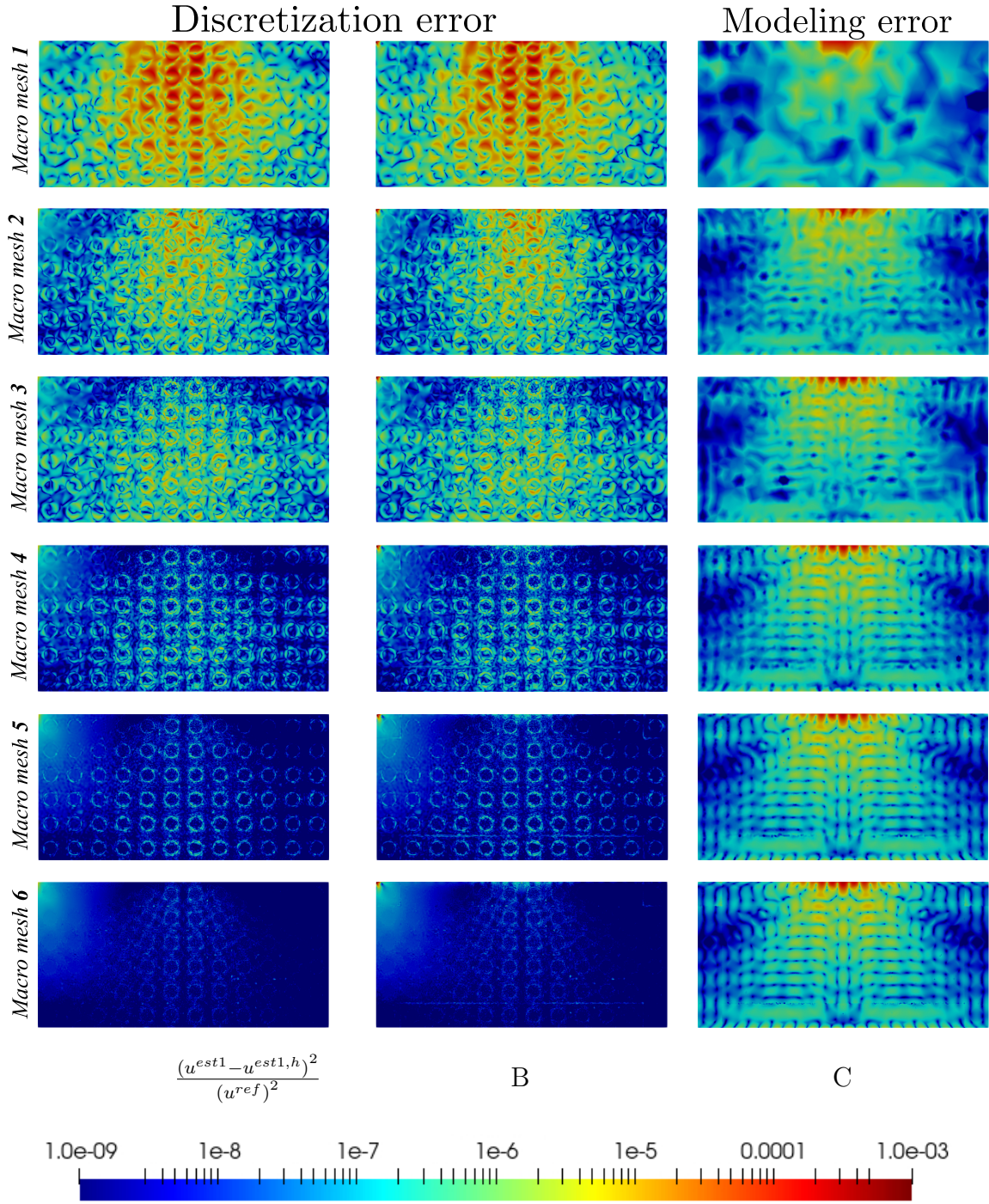


Figure 9: Comparison of relative point-wise contributions to modeling and discretization errors for a ratio $\frac{E_f}{E_m} = 10$ on different macroscale meshes illustrated in Figure 5.

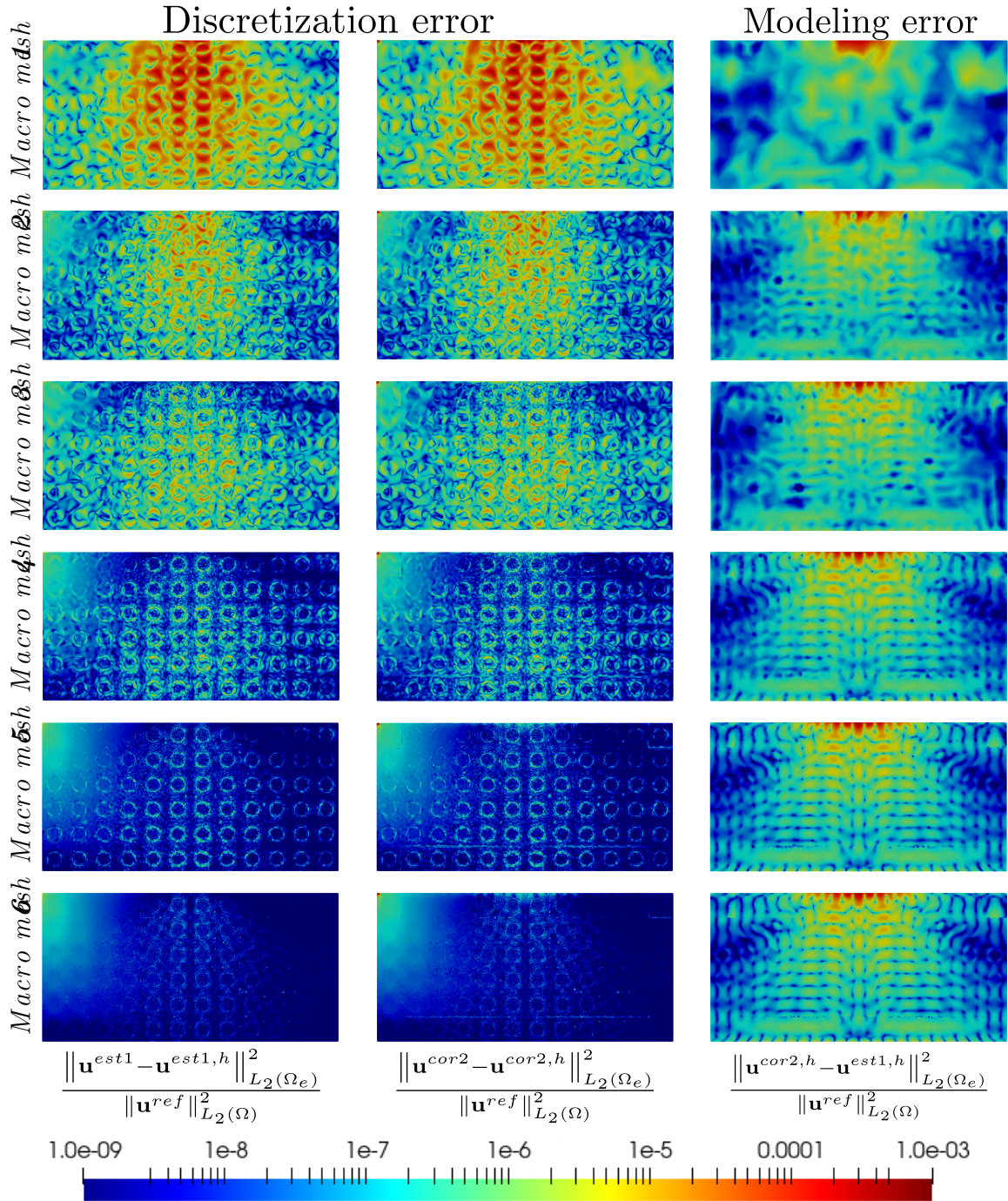


Figure 10: Comparison of relative point-wise contributions to modeling and discretization errors for a ratio $\frac{E_f}{E_m} = 500$ on different macroscale meshes illustrated in Figure 5.

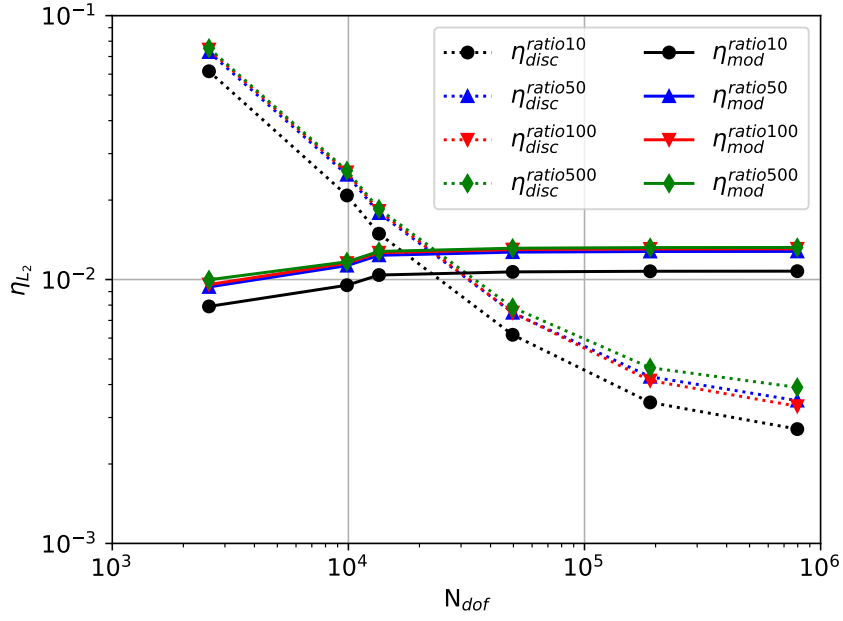
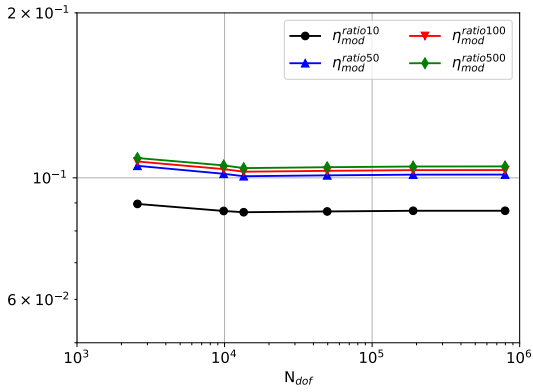
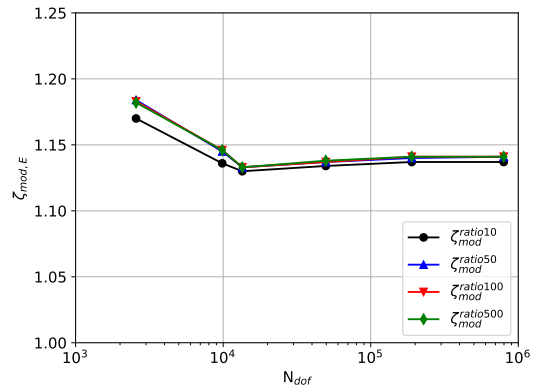


Figure 11: Global relative discretization error $\eta_{disc,rel}$ and modeling error $\eta_{mod,rel}$ on the L^2 norm of the displacement as a function of the mesh size for different ratios $\frac{E_f}{E_m}$



(a) Global relative modeling error $\eta_{mod,rel}$



(b) Effectivity index ζ_{mod}

Figure 12: Global relative modeling error $\eta_{mod,rel}$ in energy norm (12a) and corresponding effectivity index ζ_{mod} (12b) as a function of the mesh size for different ratios $\frac{E_f}{E_m}$

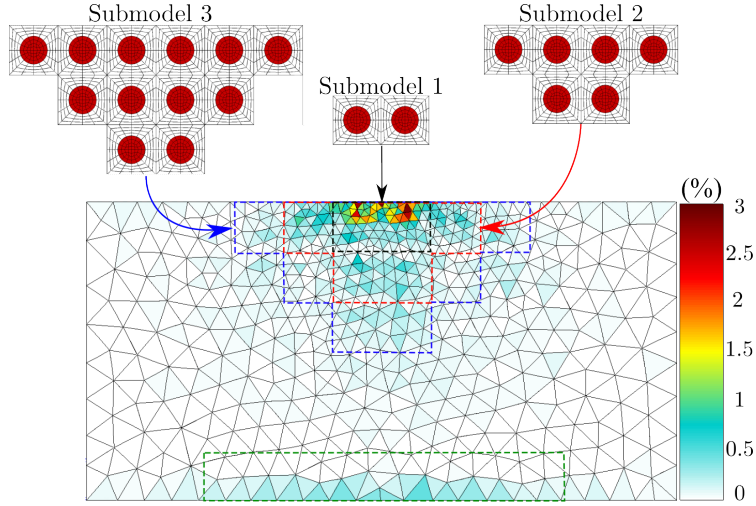


Figure 13: Relative modeling error estimation of the stress field $\frac{\|\sigma^{cor2} - \sigma^{est1}\|_{L_2(\Omega_e)}}{\|\sigma^{ref}\|_{L_2(\Omega)}}$ on macroscale mesh 3, shown in Figure 5c, and for a ratio $\frac{E_f}{E_m} = 500$. Different submodels are detected depending on target accuracy. For the sake of conciseness, the modeling error in the fixed boundary region (highlighted in green) is neglected.

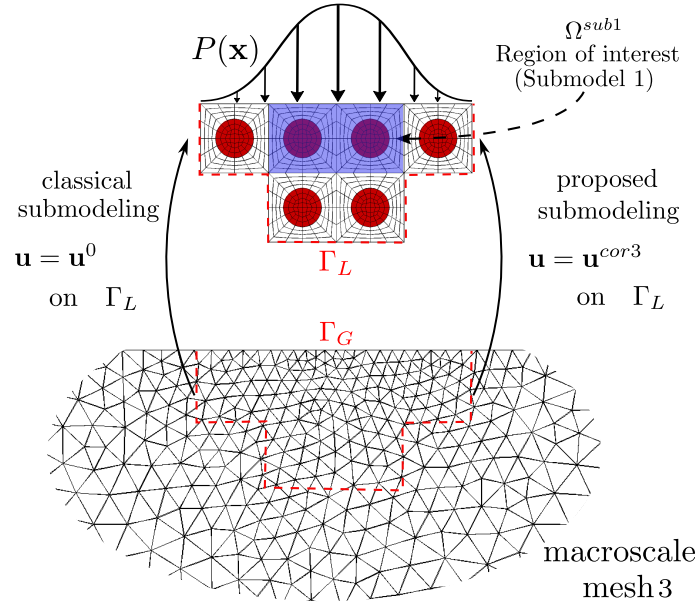
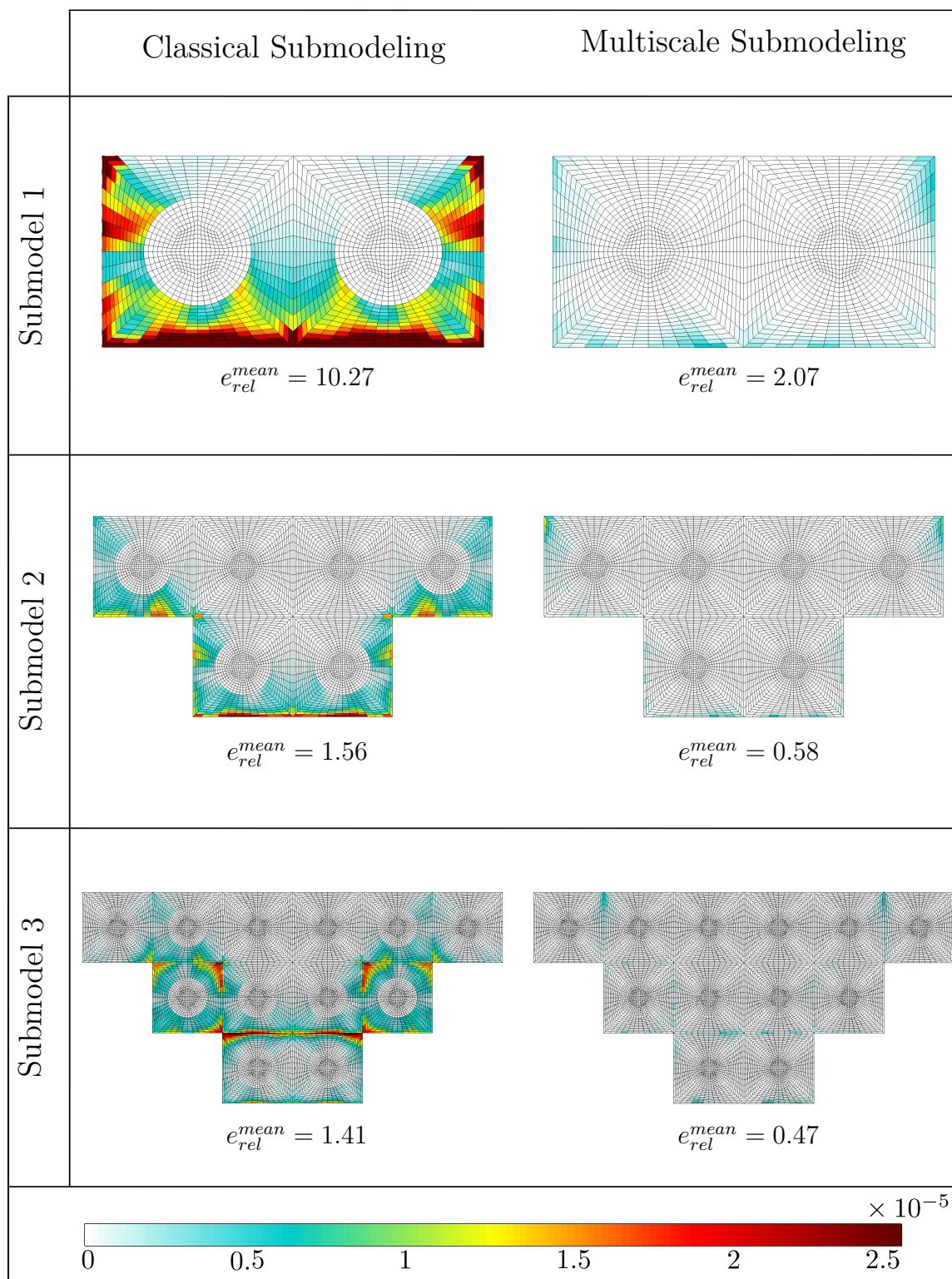


Figure 14: Illustration of the classical and the proposed submodeling techniques.



38

Figure 15: Comparison, for a ratio $\frac{E_f}{E_m} = 500$, of the element-wise relative error $e_{rel,e}$ defined in Equation 17 and the relative mean error e_{rel}^{mean} (%) defined in Equation 19, both obtained by using the classical submodeling and the proposed multiscale submodeling. The macromesh 3 (illustrated in Figure 5c) is used for the macroscale computation and the localization process.

Macroscopic mesh 1
 Macroscopic mesh 2
 Macroscopic mesh 3
 Macroscopic mesh 4
 Macroscopic mesh 5
 Macroscopic mesh 6

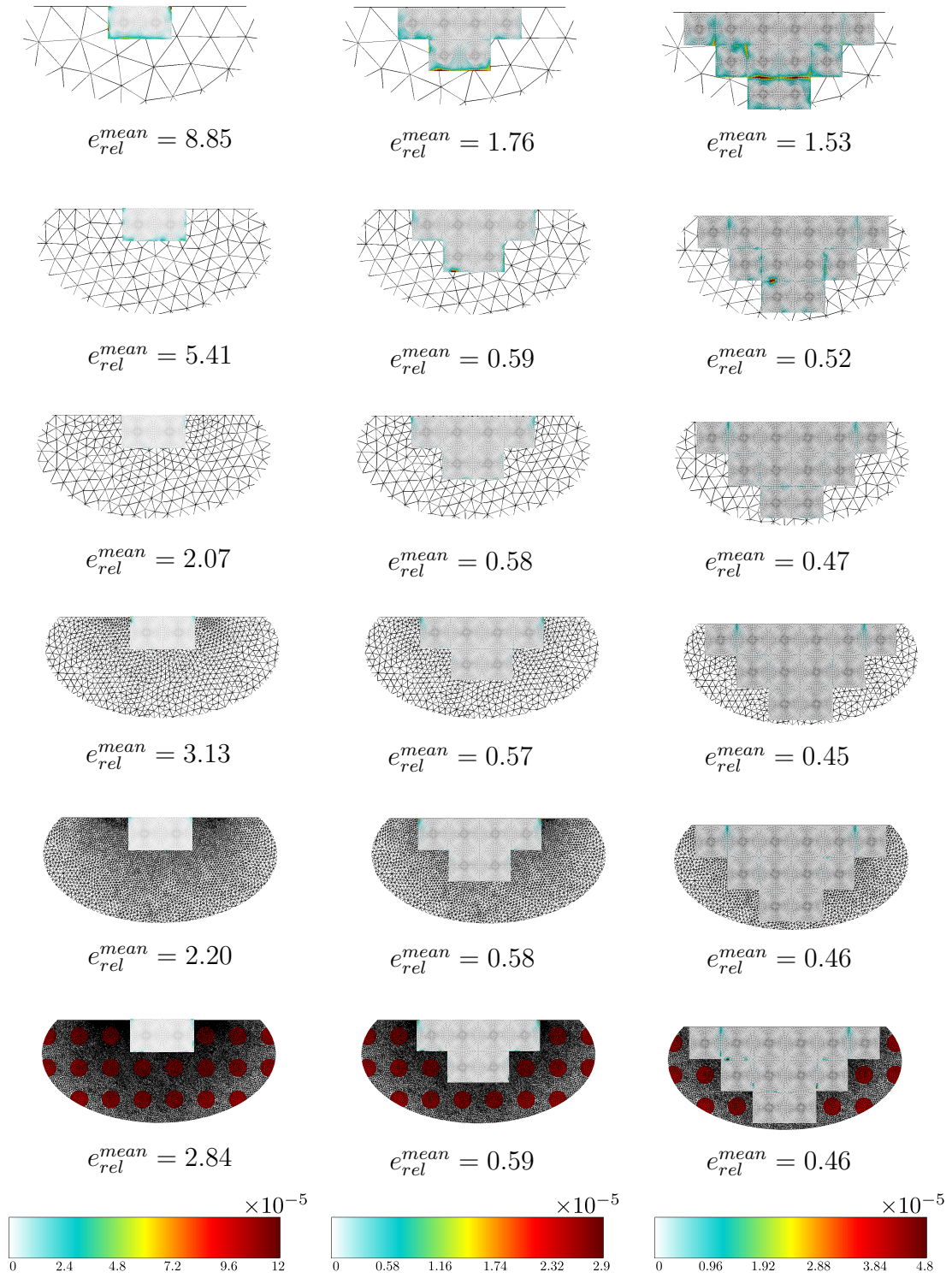


Figure 16: Comparison of the element-wise relative error $e_{rel,e}$ defined in Equation 17 and the relative mean error e_{rel}^{mean} (%) defined in Equation 19 obtained for the proposed multiscale coupling with different macroscopic meshes, for different submodels and for a ratio $\frac{E_f}{E_m} = 500$.

The main features of these results are the following:

- Classical submodeling is almost insensitive to the macroscale mesh. Indeed, the coupling error remains high even after refining the macroscale mesh, irrespective of the submodeling domain size. This is explained by the fact that the homogenized displacement field, applied on the interface of the submodel, is nearly the same for the six macroscale computations as it does not consider the microscale details, but depends only on the effective behavior, unchanged for the six macroscale computations. On the other hand, the proposed coupling is sensitive to the macroscale mesh since the localization process depends on this one.
- The proposed multiscale submodeling, with macroscale mesh 1 and 2, is significantly less accurate than with other meshes, since the localization process is still largely incorrect, as shown in Figures 6, 7, and 11.
- For all the considered cases, the relative local coupling error induced by the proposed submodeling is significantly smaller than the error obtained by the classical submodeling.
- The mean error e_{rel}^{mean} is reduced, besides results obtained for mesh 1, by at least a factor of 2 (for mesh 2 - submodel 1) and at the best by a factor of 5 (for mesh 3 - submodel 1).

A comparison of the global relative error and the relative mean error obtained for a coupling with different macroscale meshes, and for different submodels are shown in Figure 17 and Figure 18.

The main features of these results are the following:

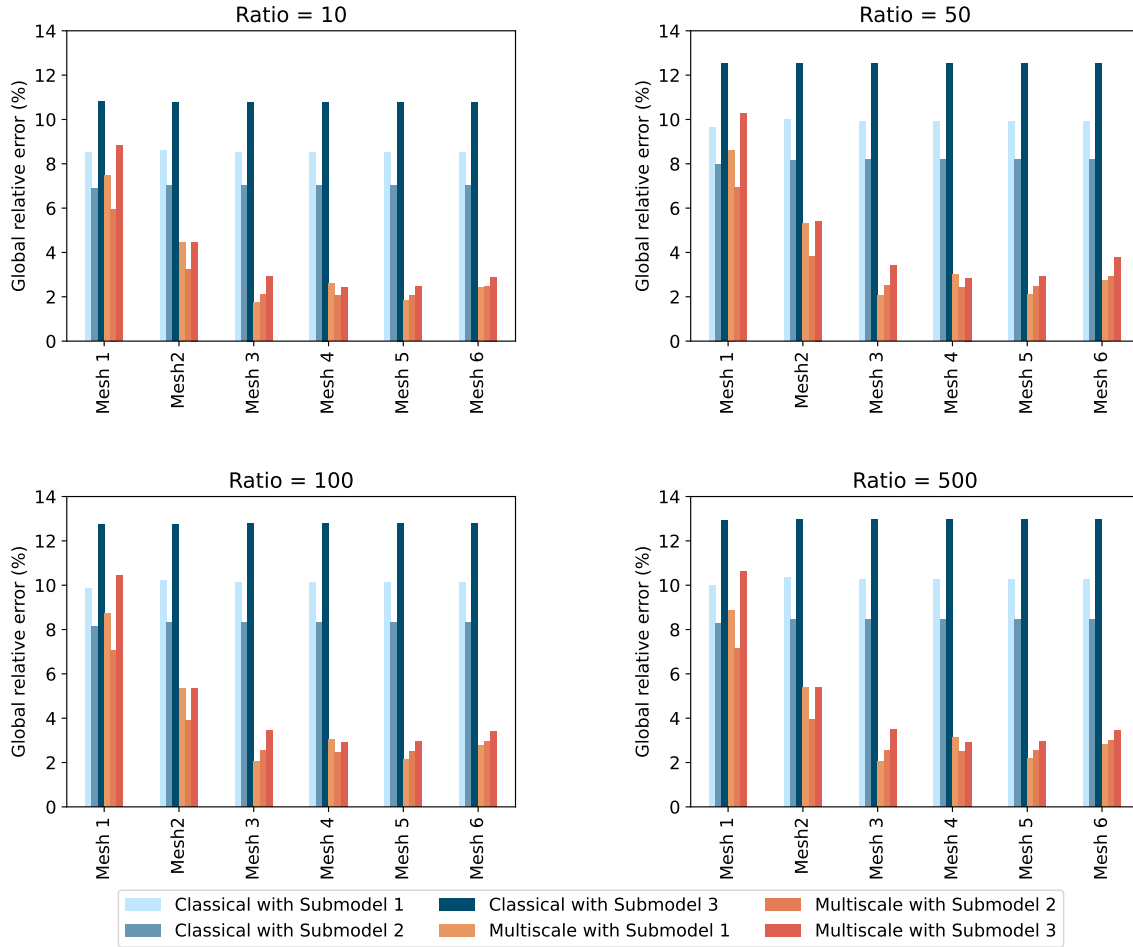


Figure 17: Comparison of the global relative error e_{rel,e_1} , defined in Equation 16, obtained for a coupling with different macroscale meshes, and for different submodels.

- The global and the mean error induced by the classical submodeling are insensitive to macroscale mesh refinement. Contrarily, the errors induced by the proposed submodeling are sensitive to the macroscale mesh refinement since the localization process is conducted on this one.

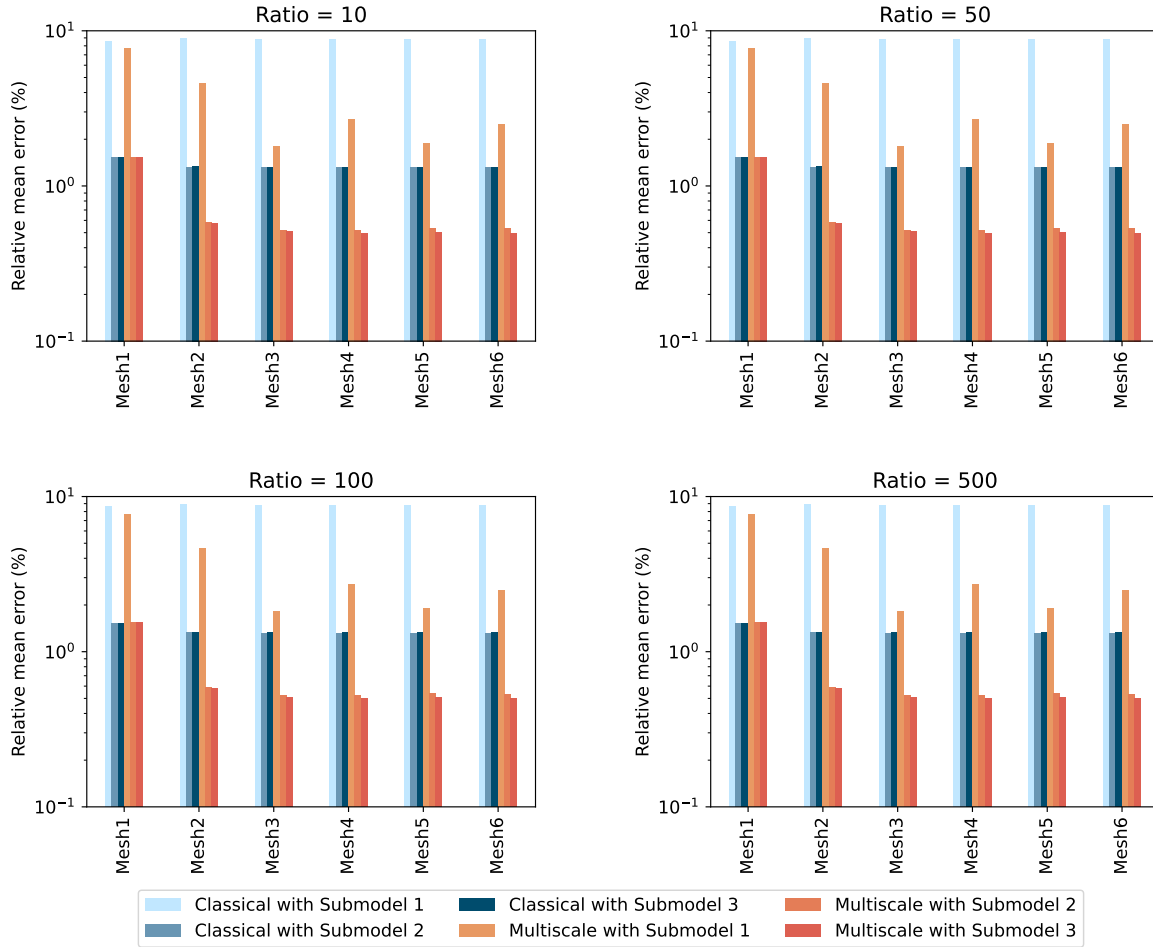


Figure 18: Comparison of the relative mean error e_{rel}^{mean} (%), defined in Equation 19, obtained for a coupling with different macroscale meshes, and for different submodels.

- For all the considered cases, the global error induced by the proposed submodeling is inferior to the one obtained by the classical submodeling. The error is reduced at least by a factor of 1.2 and the best by a factor of 5.
- The mean error in the region of interest Ω^{sub1} decreases by increasing the size

of the submodel.

- For all the considered cases, the mean error induced by the proposed submodeling is less than the one obtained by the classical submodeling. The error is reduced at least by a factor of 1.12 and the best by a factor of 5.

6. Conclusions

In this work, we have proposed a new numerical method to conduct, on a macroscale coarse mesh, a higher-order localization process to estimate local heterogeneous fields within a structure, without conducting any Direct Numerical Simulations (DNS). This localization process, contrary to first-order homogenization, takes into account additional terms of the asymptotic expansion, and thus captures the effect of macroscopic successive gradients, generally high in cases of low scale separation. The proposed localization process also includes a boundary layer correction to correct estimated fields on the boundaries. As a result, the proposed numerical method provides valuable insights on microscale fields, for a given macroscale state computed solely on the coarse macroscale mesh, much less computationally expensive than DNS.

We have also proposed a modeling error estimation based on the resulting fields computed by the aforementioned localization process. Indeed, the suggested error estimation quantifies the terms neglected by the first-order asymptotic expansion. These terms are generally significant in cases where scales are not well separated and necessary to capture gradients of the macroscale fields. The proposed error estimation is also able to quantify the modeling error on the boundaries due to the loss of periodicity assumptions in boundary regions. This modeling error estimation is used to steer a hierarchical modeling process by detecting areas where refining the material model is necessary.

To couple the microscale domain with the macroscale one, we have suggested a multiscale enhanced submodeling based on the constructed local fields. As a result, the proposed submodeling, contrary to the classical one, considers the heterogeneous nature of the submodel and remains valid in regions with low scale separation, *e.g.*

regions with high macroscale strain or stress gradients, and in the vicinity of the boundaries.

The major conclusions that can be drawn from this work are:

- The quality of the estimated stress field increases by refining the macroscale mesh. Nevertheless, it has been shown that the proposed localization process conducted on a macroscale mesh containing 113 times fewer degrees of freedom than the DNS already provides an acceptable estimation of the local stress field, as illustrated in Figures 6, and 7.
- It is possible to reduce the discretization error by refining the macroscale mesh; the modeling error, however, remains unchanged, as shown in Figure 11. To reduce this error, a hierarchical modeling can be considered.
- Classical submodeling is less sensitive to macroscale mesh refinement, contrary to the proposed submodeling, as illustrated in Figure 17 and 18.
- The proposed submodeling technique reduces the global coupling error by a factor of 5, compared to the classical submodeling, as shown in Figure 17. It also reduces the mean error in a region of interest by a factor of 5, as shown in Figure 18.

Reliable hierarchical modeling requires a feedback from the submodel computation toward the macroscale one, which has not been investigated in this work. The suggested methods could also be a path toward hierarchical modeling of realistic 3D composite structures. This implies the use of irregular structure domains, locally nonperiodic zones, and controlling simultaneously both the discretization and the modeling error.

Finally, while the extension of asymptotic homogenization to nonlinear problems is possible using incrementally linearized solutions [Bhattacharyya et al. \(2020\)](#), the derivation of a reliable estimator based on nonlinear analyses led at two different scales is far from trivial.

Declaration of competing interest

The authors declare that they have no known competing financial interests or personal relationships that could have appeared to influence the work reported in this paper.

Acknowledgments

This work was supported by the French National Association for Research and Technology (ANRT) through the research grant CIFRE 2019/1715.

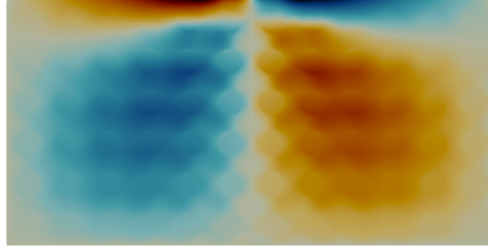
Appendix A: Comparison of localized fields on macroscale meshes

Comparison of U_1 , U_2 and σ_{11} components, solution of the problem detailed in Subsection 3.2, are presented in Figures A.1, A.2 and A.3, respectively. Same conclusions as in Subsection 3.2 are drawn. Indeed, the quality of estimated fields increases by refining the macroscale mesh. However, contribution of different material phases (matrix and fibers) to estimated fields begins to be clearly distinguished starting from mesh 3, which provides an acceptable estimation. It is also capable of capturing high gradients developed near the region where the load is applied and on the interfaces.

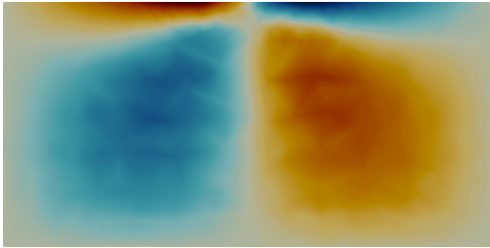
Appendix B: Comparison of the reference fields with the localized ones.

Figure B.4 shows a comparison of the reference solution \mathbf{u}^{ref} , with the obtained localized fields, \mathbf{u}^{est1} and \mathbf{u}^{cor2} for different ratios $\frac{E_f}{E_m}$. This comparison was conducted by considering an identical macroscale mesh with the microscale one. The second-order localized field corrected at the boundaries \mathbf{u}^{cor2} , highly reduces the modeling error compared to the first-order localized field \mathbf{u}^{est1} . As a result, \mathbf{u}^{cor2} provides a better estimation to \mathbf{u}^{ref} than \mathbf{u}^{est1} .

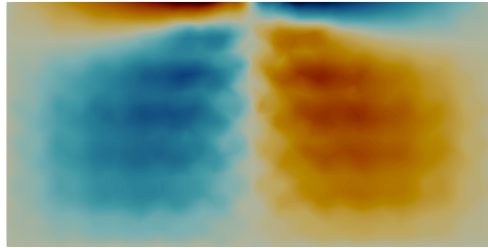
A third-order localization is supposed to provide a better solution than \mathbf{u}^{cor2} as illustrated in Fergoug et al. (2022b), albeit at a higher computational cost. We have chosen to restrict our study to \mathbf{u}^{cor2} since it is sufficient to illustrate our purpose.



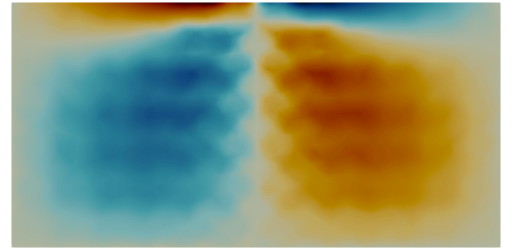
(a) U_1^{ref} on microscale mesh



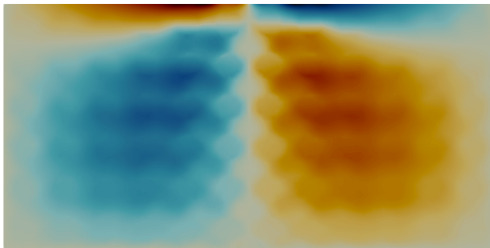
(b) U_1^{cor2} on macroscale mesh 1



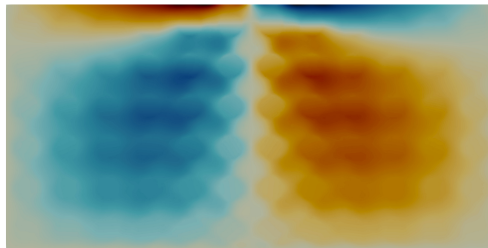
(c) U_1^{cor2} on macroscale mesh 2



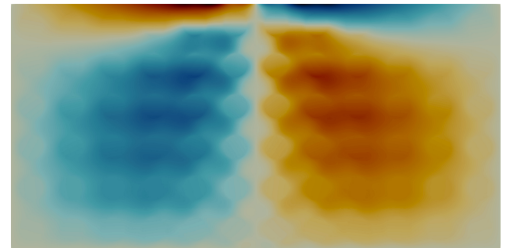
(d) U_1^{cor2} on macroscale mesh 3



(e) U_1^{cor2} on macroscale mesh 4



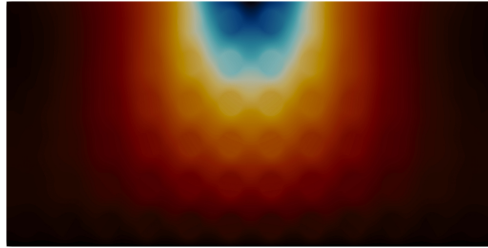
(f) U_1^{cor2} on macroscale mesh 5



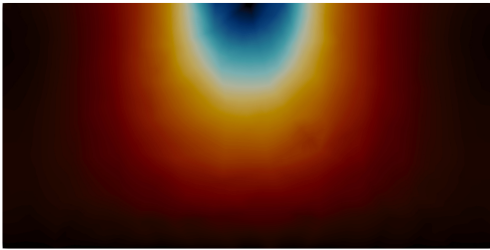
(g) U_1^{cor2} on macroscale mesh 6



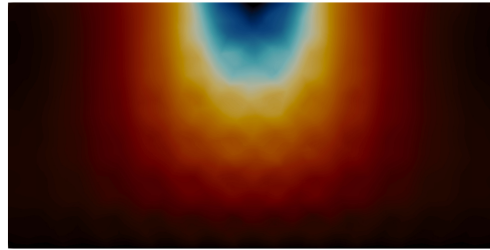
Figure A.1: Comparison of U_1 (mm) results.



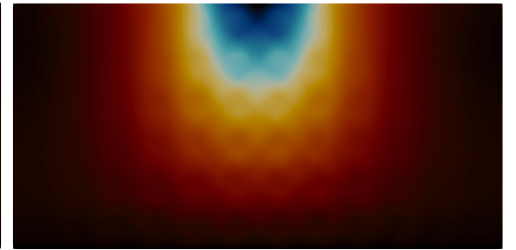
(a) U_2^{ref} on microscale mesh



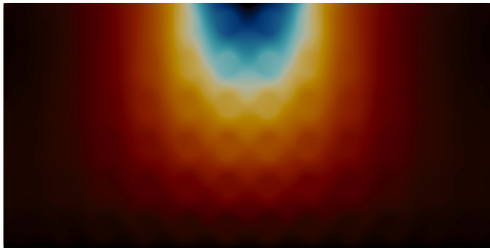
(b) U_2^{cor2} on macroscale mesh 1



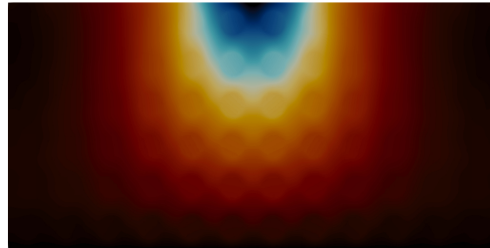
(c) U_2^{cor2} on macroscale mesh 2



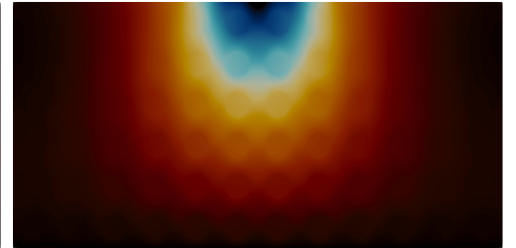
(d) U_2^{cor2} on macroscale mesh 3



(e) U_2^{cor2} on macroscale mesh 4



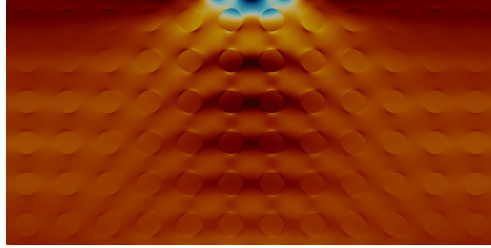
(f) U_2^{cor2} on macroscale mesh 5



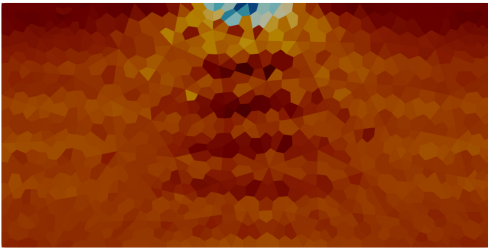
(g) U_2^{cor2} on macroscale mesh 6



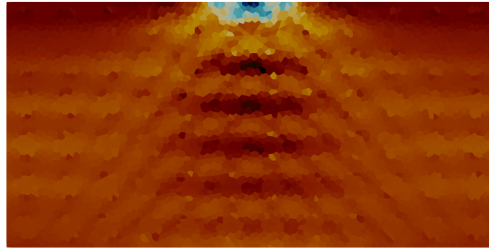
Figure A.2: Comparison of U_2 (mm) results.



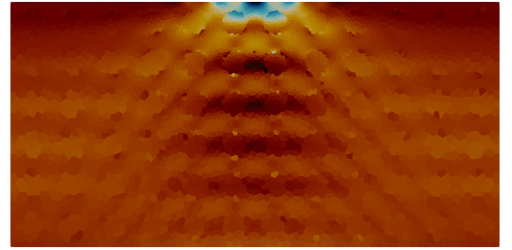
(a) σ_{11}^{ref} on microscale mesh



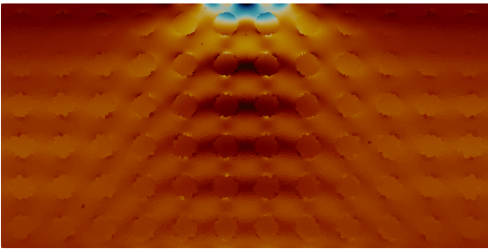
(b) σ_{11}^{cor2} on macroscale mesh 1



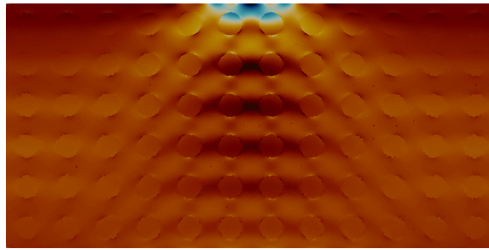
(c) σ_{11}^{cor2} on macroscale mesh 2



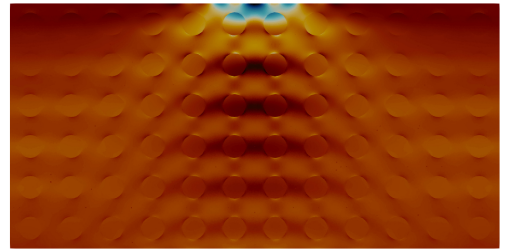
(d) σ_{11}^{cor2} on macroscale mesh 3



(e) σ_{11}^{cor2} on macroscale mesh 4



(f) σ_{11}^{cor2} on macroscale mesh 5



(g) σ_{11}^{cor2} on macroscale mesh 6

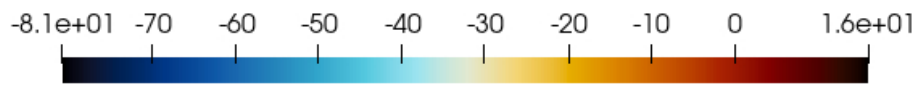


Figure A.3: Comparison of σ_{11} (MPa) results.

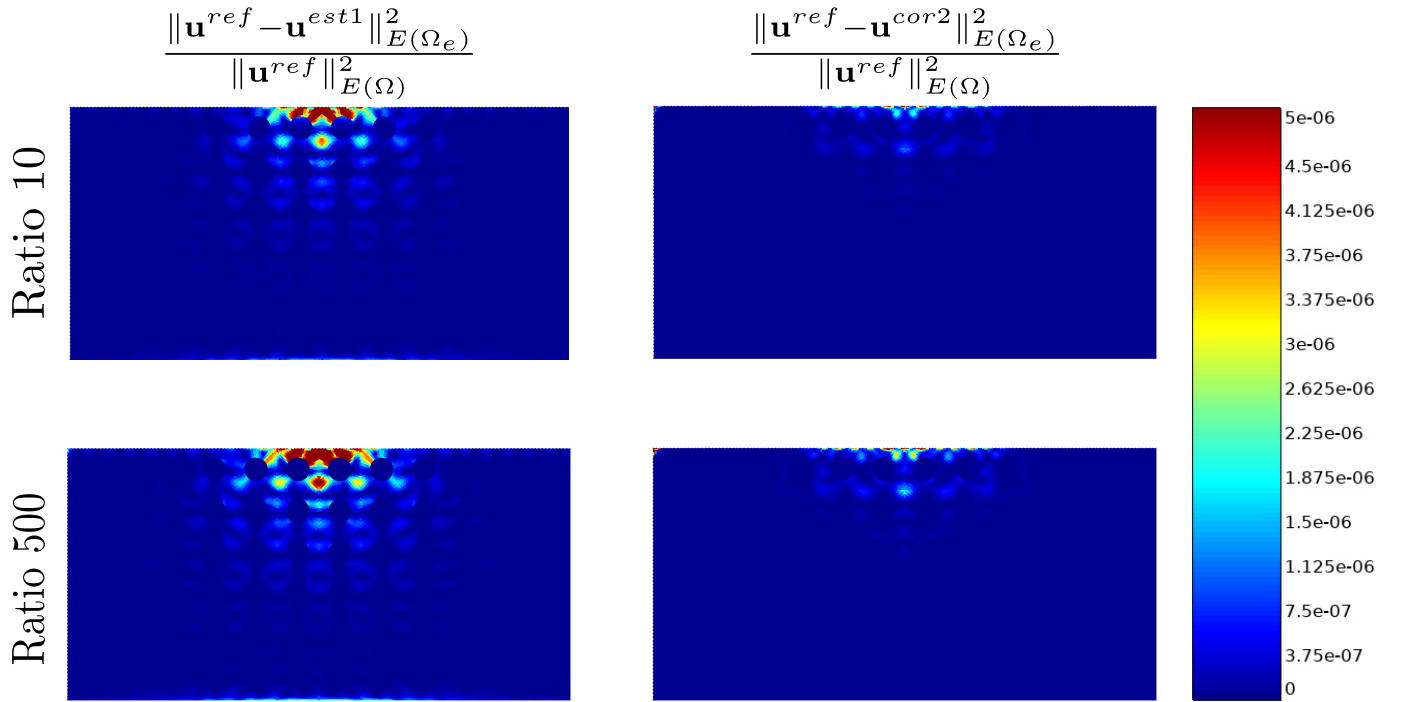


Figure B.4: Comparison of the relative local error (in the energy norm defined in Equation 14) between \mathbf{u}^{ref} and the obtained localized fields, \mathbf{u}^{est1} and \mathbf{u}^{cor2} , for different ratios $\frac{E_f}{E_m}$.

References

- Abali, B.E., Barchiesi, E., 2020. Additive manufacturing introduced substructure and computational determination of metamaterials parameters by means of the asymptotic homogenization. *Continuum Mechanics and Thermodynamics* doi:[10.1007/s00161-020-00941-w](https://doi.org/10.1007/s00161-020-00941-w).
- Abali, B.E., Vazic, B., Newell, P., 2022. Influence of microstructure on size effect for metamaterials applied in composite structures. *Mechanics Research Communications* 122, 103877.
- Ameen, M., Peerlings, R., Geers, M., 2018. A quantitative assessment of the scale separation limits of classical and higher-order asymptotic homogenization. *European Journal of Mechanics - A/Solids* 71, 89–100.
- Amini, A.M., Dureisseix, D., Cartraud, P., 2009. Multi-scale domain decomposition method for large-scale structural analysis with a zooming technique: Application to plate assembly. *International Journal for Numerical Methods in Engineering* 79, 417–443.
- Bensoussan, A., Lions, J.L., Papanicolaou, G., 2011. Asymptotic analysis for periodic structures. volume 374. American Mathematical Soc.
- Bernardi, C., Maday, Y., Rapetti, F., 2005. Basics and some applications of the mortar element method. *GAMM-Mitteilungen* 28, 97–123.
- Bhattacharyya, M., Dureisseix, D., Faverjon, B., 2020. Numerical homogenisation based on asymptotic theory and model reduction for coupled elastic-viscoplastic damage. *International Journal of Damage Mechanics* 29, 1416–1444. doi:[10.1177/1056789520930785](https://doi.org/10.1177/1056789520930785).

- Boutin, C., 1996. Microstructural effects in elastic composites. *International Journal of Solids and Structures* 33, 1023–1051.
- Dhia, H.B., 1998. Multiscale mechanical problems: the Arlequin method. *Comptes Rendus de l'Académie des Sciences Series IIB Mechanics Physics Astronomy* 12, 899–904.
- Dumontet, H., 1986. Study of a boundary layer problem in elastic composite materials. *ESAIM: Mathematical Modelling and Numerical Analysis* 20, 265–286.
- Dureisseix, D., Bavestrello, H., 2006. Information transfer between incompatible finite element meshes: application to coupled thermo-viscoelasticity. *Computer Methods in Applied Mechanics and Engineering* 195, 6523–6541.
- Fergoug, M., Parret-Fréaud, A., Feld, N., Marchand, B., Forest, S., 2022a. A general boundary layer corrector for the asymptotic homogenization of elastic linear composite structures. *Composite Structures* 285, 115091.
- Fergoug, M., Parret-Fréaud, A., Feld, N., Marchand, B., Forest, S., 2022b. Multiscale analysis of composite structures based on higher-order asymptotic homogenization with boundary layer correction. *European Journal of Mechanics - A/Solids* 96, 104754.
- Feyel, F., Chaboche, J., 2001. Multi-scale non-linear FE2 analysis of composite structures: damage and fiber size effects. *Revue Européenne des Eléments Finis* 10, 449–472. doi:[10.1080/12506559.2001.11869262](https://doi.org/10.1080/12506559.2001.11869262).
- Feyel, F., Chaboche, J.L., 2000. FE2 multiscale approach for modelling the elastoviscoplastic behaviour of long fibre SiC/Ti composite materials. *Computer methods in applied mechanics and engineering* 183, 309–330.

- Fish, J., Belsky, V., 1995. Multi-grid method for periodic heterogeneous media part 2: Multiscale modeling and quality control in multidimensional case. *Computer Methods in Applied Mechanics and Engineering* 126, 17–38.
- Fish, J., Markolefas, S., 1993. Adaptive s-method for linear elastostatics. *Computer Methods in Applied Mechanics and Engineering* 104, 363–396.
- Fish, J., Markolefas, S., Guttal, R., Nayak, P., 1994a. On adaptive multilevel superposition of finite element meshes for linear elastostatics. *Applied Numerical Mathematics* 14, 135–164.
- Fish, J., Nayak, P., Holmes, M.H., 1994b. Microscale reduction error indicators and estimators for a periodic heterogeneous medium. *Computational Mechanics* 14, 323–338.
- Fish, J., Shek, K., 2000. Multiscale analysis of composite materials and structures. *Composites Science and Technology* 60, 2547–2556.
- Fish, J., Yu, Q., 2001. Multiscale damage modelling for composite materials: theory and computational framework. *International Journal for Numerical Methods in Engineering* 52, 161–191.
- Ghosh, S., Bai, J., Raghavan, P., 2007. Concurrent multi-level model for damage evolution in microstructurally debonding composites. *Mechanics of Materials* 39, 241–266.
- Ghosh, S., Lee, K., Moorthy, S., 1995. Multiple scale analysis of heterogeneous elastic structures using homogenization theory and voronoi cell finite element method. *International Journal of Solids and Structures* 32, 27–62.

- Ghosh, S., Lee, K., Raghavan, P., 2001. A multi-level computational model for multi-scale damage analysis in composite and porous materials. *International Journal of Solids and Structures* 38, 2335–2385.
- Guedes, J., Kikuchi, N., 1990. Preprocessing and postprocessing for materials based on the homogenization method with adaptive finite element methods. *Computer Methods in Applied Mechanics and Engineering* 83, 143–198.
- Hassani, B., Hinton, E., 2012. Homogenization and structural topology optimization: theory, practice and software. Springer Science & Business Media.
- He, Z., Pindera, M.J., 2020. Finite volume-based asymptotic homogenization of periodic materials under in-plane loading. *Journal of Applied Mechanics* 87, 121010.
- Hollister, S.J., Kikuchi, N., 1992. A comparison of homogenization and standard mechanics analyses for periodic porous composites. *Computational mechanics* 10, 73–95.
- Josien, M., 2019. Some quantitative homogenization results in a simple case of interface. *Communications in Partial Differential Equations* 44, 907–939. doi:[10.1080/03605302.2019.1610892](https://doi.org/10.1080/03605302.2019.1610892).
- Kanouté, P., Boso, D.P., Chaboche, J.L., Schrefler, B.A., 2009. Multiscale Methods for Composites: A Review. *Archives of Computational Methods in Engineering* 16, 31–75.
- Kouznetsova, V., Brekelmans, W., Baaijens, F., 2001. An approach to micro-macro modeling of heterogeneous materials. *Computational mechanics* 27, 37–48.

- Kouznetsova, V., Geers, M.G., Brekelmans, W.M., 2002. Multi-scale constitutive modelling of heterogeneous materials with a gradient-enhanced computational homogenization scheme. *International Journal for Numerical Methods in Engineering* 54, 1235–1260.
- Kruch, S., Forest, S., 1998. Computation of coarse grain structures using a homogeneous equivalent medium. *Journal de Physique IV* 08, Pr8–197–Pr8–205.
- Lloberas-Valls, O., Rixen, D., Simone, A., Sluys, L., 2012. On micro-to-macro connections in domain decomposition multiscale methods. *Computer methods in applied mechanics and engineering* 225, 177–196.
- Miehe, C., Koch, A., 2002. Computational micro-to-macro transitions of discretized microstructures undergoing small strains. *Archive of Applied Mechanics* 72, 300–317.
- Moulinec, H., Suquet, P., 1998. A numerical method for computing the overall response of nonlinear composites with complex microstructure. *Computer methods in applied mechanics and engineering* 157, 69–94.
- Oden, J., Vemaganti, K.S., 2000. Estimation of Local Modeling Error and Goal-Oriented Adaptive Modeling of Heterogeneous Materials. *Journal of Computational Physics* 164, 22–47.
- Oden, J., Zohdi, T.I., 1997. Analysis and adaptive modeling of highly heterogeneous elastic structures. *Computer Methods in Applied Mechanics and Engineering* 148, 367–391.
- Oden, J.T., Prudhomme, S., Hammerand, D.C., Kuczma, M.S., 2001. Modeling

- error and adaptivity in nonlinear continuum mechanics. *Computer Methods in Applied Mechanics and Engineering* 190, 6663–6684.
- Oden, J.T., Vemaganti, K., 1999. Adaptive modeling of composite structures: Modeling error estimation, in: *Texas Institute for Computational and Applied Mathematics*, Citeseer.
- Pipes, R.B., Kaminski, B., Pagano, N., 1973. Influence of the free edge upon the strength of angle-ply laminates, in: *Analysis of the test methods for high modulus fibers and composites*. ASTM International.
- Raghavan, P., Ghosh, S., 2004. Concurrent multi-scale analysis of elastic composites by a multi-level computational model. *Computer methods in applied mechanics and engineering* 193, 497–538.
- Raghavan, P., Li, S., Ghosh, S., 2004. Two scale response and damage modeling of composite materials. *Finite Elements in Analysis and Design* 40, 1619–1640.
- Sanchez-Palencia, E., 1983. Homogenization method for the study of composite media, in: *Asymptotic Analysis II—*. Springer, pp. 192–214.
- Sigmund, O., 1995. Tailoring materials with prescribed elastic properties. *Mechanics of Materials* 20, 351–368.
- Suzuki, K., Kikuchi, N., 1991. A homogenization method for shape and topology optimization. *Computer Methods in Applied Mechanics and Engineering* 93, 291–318.
- Tartar, L., 2009. *The general theory of homogenization*. Springer, Berlin Heidelberg. doi:[10.1007/978-3-642-05195-1](https://doi.org/10.1007/978-3-642-05195-1).

- Temizer, I., Wriggers, P., 2011. An adaptive multiscale resolution strategy for the finite deformation analysis of microheterogeneous structures. *Computer Methods in Applied Mechanics and Engineering* 200, 2639–2661.
- Terada, K., Kikuchi, N., 1995. Nonlinear homogenization method for practical applications. American Society of Mechanical Engineers, Applied Mechanics Division, AMD 212, 1–16.
- Vernerey, F.J., Kabiri, M., 2012. An adaptive concurrent multiscale method for microstructured elastic solids. *Computer Methods in Applied Mechanics and Engineering* 241-244, 52–64.
- Visroliia, A., Meo, M., 2013. Multiscale damage modelling of 3D weave composite by asymptotic homogenisation. *Composite Structures* 95, 105–113.
- Wangermez, M., Allix, O., Guidault, P.A., Ciobanu, O., Rey, C., 2020. Interface coupling method for the global–local analysis of heterogeneous models: A second-order homogenization-based strategy. *Computer Methods in Applied Mechanics and Engineering* 365, 113032.
- Yang, H., Abali, B.E., Müller, W.H., Barboura, S., Li, J., 2022. Verification of asymptotic homogenization method developed for periodic architected materials in strain gradient continuum. *International Journal of Solids and Structures* 238, 111386.
- Yang, H., Abali, B.E., Timofeev, D., Müller, W.H., 2019. Determination of metamaterial parameters by means of a homogenization approach based on asymptotic analysis. *Continuum Mechanics and Thermodynamics* doi:[10.1007/s00161-019-00837-4](https://doi.org/10.1007/s00161-019-00837-4).

- Yang, H., Timofeev, D., Giorgio, I., Müller, W.H., 2020. Effective strain gradient continuum model of metamaterials and size effects analysis. *Continuum Mechanics and Thermodynamics* doi:[10.1007/s00161-020-00910-3](https://doi.org/10.1007/s00161-020-00910-3).
- Yvonnet, J., Bonnet, G., 2014. Nonlocal/coarse-graining homogenization of linear elastic media with non-separated scales using least-square polynomial filters. *International Journal for Multiscale Computational Engineering* 12, 375–395.
- Zienkiewicz, O.C., Zhu, J.Z., 1992a. The superconvergent patch recovery and a posteriori error estimates. part 1: The recovery technique. *International Journal for Numerical Methods in Engineering* 33, 1331–1364.
- Zienkiewicz, O.C., Zhu, J.Z., 1992b. The superconvergent patch recovery and a posteriori error estimates. part 2: Error estimates and adaptivity. *International Journal for Numerical Methods in Engineering* 33, 1365–1382.
- Zohdi, T.I., Oden, J., Rodin, G.J., 1996. Hierarchical modeling of heterogeneous bodies. *Computer Methods in Applied Mechanics and Engineering* 138, 273–298.